NEUROSCIENCE

Aberrant outputs of glutamatergic neurons in deep cerebellar nuclei mediate dystonic movements

Xue-Mei Wu[1,2,3]†, Bin Lu[1]†, Jun-Yan He[1,2], Yu-Xian Zhang[1], Zhi-Ying Wu[4], Zhi-Qi Xiong[1,2,3,5]*

Dystonia, characterized by repetitive twisting movements or abnormal postures, has been linked to the deep cerebellar nuclei (DCN). However, the specific roles of distinct neuronal populations within the DCN in driving dystonic behaviors remain unclear. This study explores the contributions of three distinct groups of DCN neurons in an animal model of paroxysmal dystonia harboring a mutation in the proline-rich transmembrane protein 2 (*Prrt2*) gene. We observed sustained calcium activity elevation across glutamatergic, glycinergic, and GABAergic inferior olive (IO)–projecting neurons within the DCN during episodes of dystonia in *Prrt2*-mutant mice. However, only the optogenetic activation of DCN glutamatergic neurons, but not glycinergic or GABAergic IO-projecting neurons, elicited dystonia-like behaviors in normal mice. Selective ablation of DCN glutamatergic neurons effectively eliminated aberrant cerebellar DCN outputs and alleviated dystonia attacks in both *Prrt2*-associated and kainic acid–induced dystonia mouse models. Collectively, our findings highlight the pivotal role of aberrant activation of DCN glutamatergic neurons in the neuropathological mechanisms underlying cerebellar-originated dystonia.

INTRODUCTION

Dystonia, the third most common movement disorder behind essential tremor and Parkinson's disease, is characterized by involuntary, sustained, or intermittent muscle contractions that result in repetitive twisting movements or abnormal postures (*1*). Traditionally, dystonia was regarded as a disorder of the basal ganglia (*2*–*6*). However, recent studies have implicated cerebellar dysfunction in the pathophysiology of dystonia (*7*–*14*).

In the cerebellum, the deep cerebellar nuclei (DCN) serve as a central information hub that integrates inputs from the cerebellar cortex and extracerebellar brain regions and sends primary outputs to motor control systems (*15*). Accumulating evidence supports the involvement of DCN neurons in dystonic movements. In animal models of dystonia, DCN neurons often exhibited erratic firing patterns during attacks (*7*, *9*, *10*, *12*, *13*, *16*, *17*). Lesion or targeted interventions in the DCN such as deep brain stimulation (DBS) or pharmacological modulation alleviate dystonia symptoms (*11*, *12*, *16*, *18*–*20*). In wild-type mice, both intense activation and inhibition of DCN neurons by artificial manipulations can directly induce dystonia-like behaviors (*16*, *17*), supporting their dominant role in generating dystonic movements.

The DCN are composed of at least three neuronal populations, including glutamatergic, glycinergic, and γ-aminobutyric acid (GABA)–releasing neurons (*21*, *22*). Although the circuit connections of these neurons in the DCN have been mapped (*23*, *24*) and the neuronal functions in motor coordination were partially elucidated (*25*–*27*), their exact roles in mediating dystonic movements remain unclear.

In the present study, we used an animal model of paroxysmal dystonia, *Prrt2*-mutant mice, to dissect the roles of distinct DCN neuronal groups in dystonia. These mutant mice harbor a premature termination codon in exon 2 of the proline-rich transmembrane protein 2 (*Prrt2*) gene, which mirrors the *PRRT2* mutation identified in human patients with paroxysmal kinesigenic dyskinesia (PKD). They exhibit dystonic episodes partially recapitulating the involuntary movements and abnormal postures observed in patients with PKD (*28*). Our previous studies have shown that spontaneous dystonic episodes in *Prrt2*-mutant mice are exceedingly rare, but these symptoms can be reliably induced by localized cerebellar stimulation (*17*, *28*), making the *Prrt2*-mutant mice a valuable and inducible model for paroxysmal dystonia research.

Here, using cell-type–specific fiber photometry recording, optogenetic manipulation, and selective neuron ablation, we investigated the causal relationships between the activities of different DCN neuronal groups and dystonic movements and further identified the potential targets for the prevention of dystonia attacks in animal models of paroxysmal dystonia.

RESULTS

DCN neurons with sustained elevated activities during episodes of dystonia

In *Prrt2*-mutant mice, the deficiency of PRRT2 increases the excitability of cerebellar granule cells, rendering the cerebellar cortex more susceptible to the generation of spreading depolarization (SD) (*17*). Localized cerebellar stimulation, such as epidural KCl application or optogenetic stimulation, has been effectively used to induce cerebellar SD. This event is considered a pivotal trigger for paroxysmal dystonia in *Prrt2*-mutant mice, as demonstrated in previous studies (*17*). In this study, electrostimulation was used to induce dystonic movements in *Prrt2*-mutant mice by triggering a slowly propagated SD in the cerebellar cortex, as indicated by the direct current (dc)–shift signals detected through full-band electrocorticographic (ECoG) recording (fig. S1, A to C). Metal electrodes were implanted into the seventh cerebellar lobule (Cb) to deliver the stimulation (Fig. 1A). Following a 2.5-s pulsed electrostimulation at 200 μA (1-ms pulse width at 20 Hz), paroxysmal dystonia was observed in all *Prrt2*-mutant mice, but not in their wild-type counterparts (Fig. 1, B

[1]Institute of Neuroscience, CAS Center for Excellence in Brain Science and Intelligence Technology, Chinese Academy of Sciences, Shanghai 200031, China. [2]University of Chinese Academy of Sciences, Beijing 100049, China. [3]School of Life Science and Technology, ShanghaiTech University, Shanghai 201210, China. [4]Department of Medical Genetics and Center for Rare Diseases, Second Affiliated Hospital, Zhejiang University School of Medicine and Zhejiang Key Laboratory of Rare Diseases for Precision Medicine and Clinical Translation, Hangzhou, Zhejiang 310009, China. [5]Shanghai Center for Brain Science and Brain-Inspired Intelligence Technology, Shanghai 201210, China.
*Corresponding author. Email: xiongzhiqi@ion.ac.cn
†These authors contributed equally to this work.

and C). These dystonic behaviors are distinct from seizures, as no epileptic activity was detected in ECoG recording in the cerebral cortex during dystonic movements (fig. S2, A to D). The episodes in *Prrt2*-mutant mice were characterized by generalized dystonia, including rigid forelimbs, slow elevation of the tail, flattening of the trunk, excessive extension of the hindlimbs, and backward stretching of the ears (movie S1). Notably, the dystonic movements or postures often occurred after a variable latent period (86.6 ± 4.9 s) and lasted for ~2 min (135.2 ± 12.1 s) (Fig. 1, D and E), consistent with previous reports (*17*). Quantitative assessment of dystonia severity, as outlined in Materials and Methods, highlighted the characteristic dystonia attacks in *Prrt2*-mutant mice (Fig. 1F).

Furthermore, we confirmed that dystonic behaviors could be elicited in *Prrt2*-mutant mice by applying electrostimulation to the fourth and fifth Cbs (fig. S3, A to F). The latency to the onset of dystonic behaviors was shorter compared to that observed in *Prrt2*-mutant mice receiving electrostimulation in the seventh Cb (Fig. 1D and fig. S3D). These findings indicate that dystonic behaviors can be triggered by stimulation across various cerebellar regions, with variable latency. In the subsequent experiments, considering factors such as physical interference between the stimulation electrode and the fiber cannula, we selected seventh Cb as the target for cerebellar stimulation. This choice ensured the effective induction of dystonia in *Prrt2*-mutant mice without compromising the recording configuration.

In cerebellar circuits, the cerebellar cortex does not directly influence motor effectors. Instead, its output converged at the level of the DCN, which are situated beneath the cerebellar cortex. Rather than functioning merely as a passive relay, the DCN integrate inhibitory inputs from Purkinje cells and excitatory inputs from mossy fibers originating in precerebellar regions (*29*–*32*), thereby shaping both the temporal and spatial dynamics of cerebellar signaling (*33*–*35*). On the basis of this central integrative role, we hypothesized that neuronal activity within the DCN may be altered during episodes of dystonia in *Prrt2*-mutant mice.

To test this idea, fiber photometry was used to monitor population calcium signals in DCN neurons. Adeno-associated virus (AAV) containing the human synapsin promoter (hSyn)–GCaMP6f construct was injected into the DCN, where GCaMP6f was selectively expressed in the neurons under the control of the human synapsin promoter. We targeted the optical fiber to the interposed nucleus (IN), which is centrally located within the DCN. The stimulating electrode was positioned on the seventh Cb to avoid potential physical interference with the fiber cannula (Fig. 1, G and H). Cerebellar electrostimulation induced substantial elevations in calcium signals in head-restrained awake *Prrt2*-mutant mice, but not in the control group of wild-type mice (Fig. 1, I and J). Detectable elevation of calcium signals was often observed preceding the initiation of dystonia attacks, reaching peak intensity during severe dystonia attacks (Fig. 1I

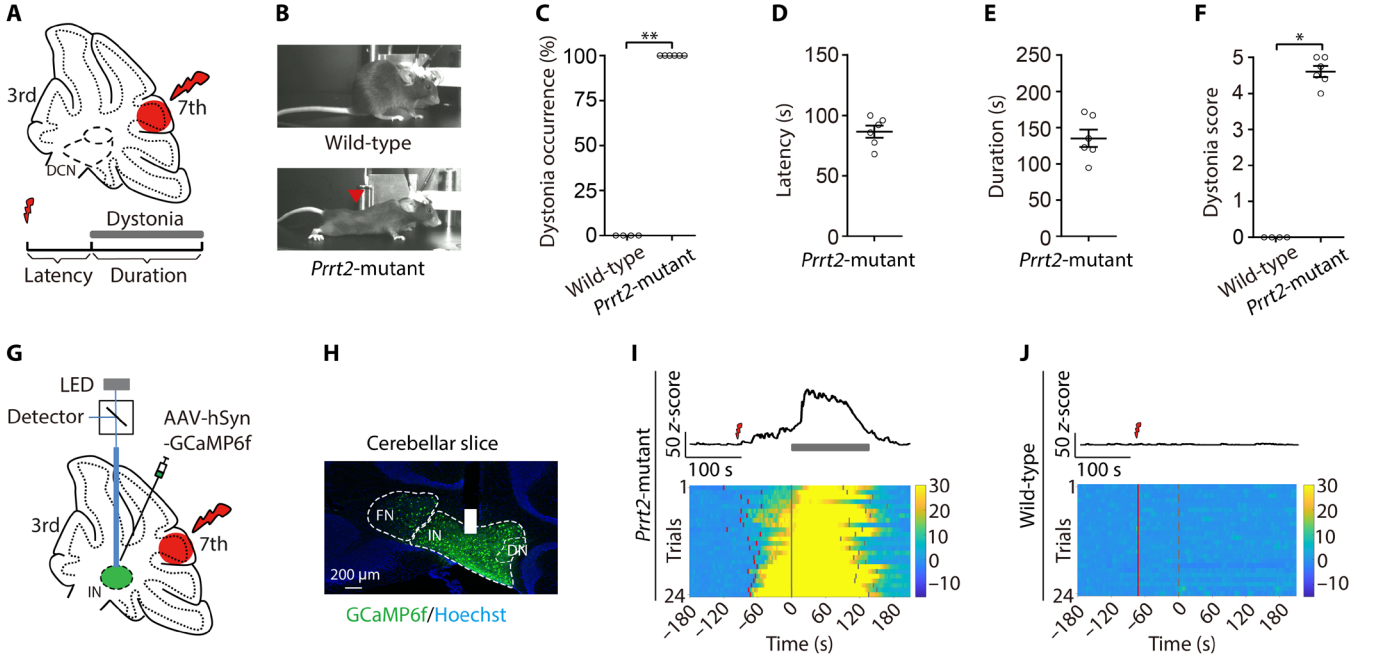

Fig. 1. DCN neurons with sustained elevated activities during episodes of dystonia. (**A**) Schematic showing electrostimulation in the localized area of the seventh Cb in mice. (**B**) Representative postures of wild-type (top) and *Prrt2*-mutant mice (bottom) following electrostimulation. Red arrowhead indicates dystonic movements. (**C**) Percentage of occurrence of dystonia triggered by electrostimulation in wild-type ($n = 4$ mice) and *Prrt2*-mutant mice ($n = 6$ mice). $^{**}P < 0.01$, Fisher's exact test (two sided). (**D**) Average latency of dystonia onset after electrostimulation in *Prrt2*-mutant mice ($n = 6$ mice). (**E**) Average duration of dystonia induced by electrostimulation in *Prrt2*-mutant mice ($n = 6$ mice). (**F**) Quantification of dystonia score in wild-type ($n = 4$ mice) and *Prrt2*-mutant mice ($n = 6$ mice). $^{*}P < 0.05$, Mann-Whitney *U* test. (**G**) Illustration showing the detection of calcium signals in the DCN. IN, interposed nucleus. LED, light-emitting diode. (**H**) Representative histological image indicating GCaMP6f expression in the DCN. Solid white column marks the location of the implanted fiber. FN, fastigial nucleus; DN, dentate nucleus. (**I** and **J**) Top: Representative calcium traces of DCN neurons in *Prrt2*-mutant (I) and wild-type (J) mice received electrostimulation in the local cerebellar cortex. Dark gray shade marks the duration of dystonia. Scale bars, 50 *z*-score by 100 s. Bottom: Heatmaps illustrating the calcium responses in DCN neurons of *Prrt2*-mutant ($n = 24$ trials from four mice) (I) and wild-type ($n = 24$ trials from four mice) (J) mice before and after the electrostimulation. The signals were aligned to the onset of dystonia. The red lines indicate the time of electrostimulation. The long dark gray lines mark the initiation of the attack in *Prrt2*-mutant mice (I) or the hypothetic onset time in wild-type mice (J). The short dark gray lines indicate the offset of dystonia. (D to F) Data were represented as means ± SEM.

and fig. S4, A and B). The increase in calcium signals endured for more than 60 s, followed by a recovery in fluorescence intensity concurrent with the alleviation of dystonia attacks (Fig. 1I and fig. S4A). These findings confirm the disrupted activation of DCN neurons during episodes of dystonia in *Prrt2*-mutant mice, suggesting a distinct role of DCN neurons in the manifestation of dystonic movements.

Increased activity in DCN^{vGlut2} neurons during dystonic episodes

Given the crucial role of glutamatergic neurons in the excitatory projection from the DCN, we examined the cellular activities of these neurons in the DCN using fiber photometry. Glutamatergic neurons are dispersed across all three nuclei of the DCN, namely, the fastigial, interposed, and dentate nuclei (*21*). Therefore, we recorded calcium signals in the DCN without discriminating among individual nuclei. In this experiment, we injected an AAV virus containing the hSyn-double floxed inverse orientation (DIO)–GCaMP6f construct into the fastigial nucleus (FN) or IN of DCN (Fig. 2A). The expression of GCaMP6f in DCN glutamatergic neurons was controlled by Cre recombinase in *vGlut2-cre* mice (*36*), where Cre recombinase expression was driven by the vesicle glutamate transporter 2 (*vGlut2*) promoter (*vGlut2-cre*::DIO-GCaMP6f) (Fig. 2, A and B).

After applying electrostimulation to the local cerebellar cortex, a substantial elevation in Ca^{2+} levels was observed in DCN glutamatergic neurons in all tested *Prrt2*-mutant mice (*Prrt2*-mutant;*vGlut2-cre*::DIO-GCaMP6f) (Fig. 2C). Aligning the fluorescence signals with the initiation of dystonic behaviors revealed a pronounced increase in calcium signals coinciding with the attacks, persisting for a duration exceeding 60 s (Fig. 2C). In a control group of wild-type mice (wild-type;*vGlut2-cre*::DIO-GCaMP6f), identical stimulation failed to provoke dystonic movements, and no comparable pattern of calcium signal changes was observed (Fig. 2D). These results suggest that the aberrant activity of DCN glutamatergic neurons is associated with episodes of dystonia.

Glutamatergic neurons within the DCN project widely to multiple brain regions, including the diencephalon, brainstem, and spinal cord, and they also send collateral outputs to several extracerebellar targets (*23*, *27*, *37*). To further assess the altered outputs of DCN glutamatergic neurons, we specifically monitored neuronal activity in one of their major targets, the ventrolateral nucleus of the thalamus (VL thalamus), as an indirect readout of DCN glutamatergic output changes during dystonic episodes.

Using calcium fiber photometry, we recorded neuronal responses in the VL thalamus of *Prrt2*-mutant mice (Fig. 2, E and F). We found

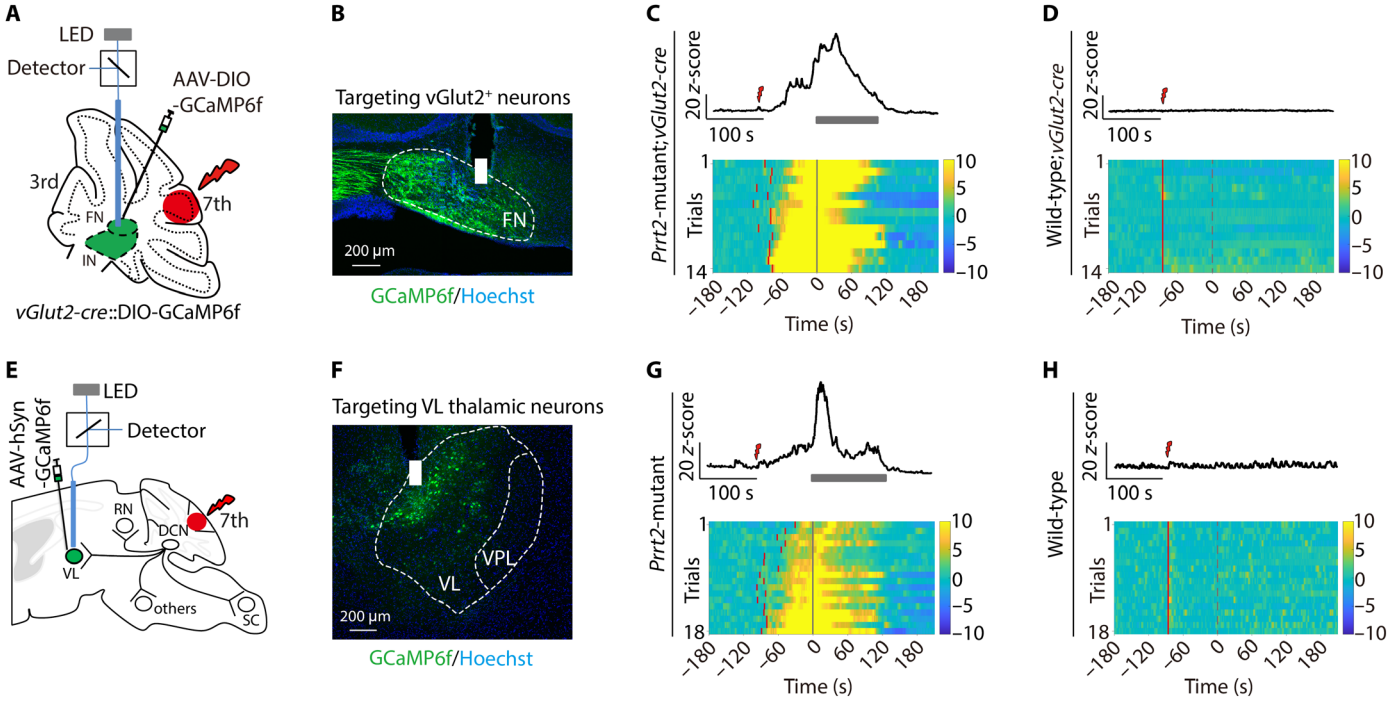

Fig. 2. Increased activity in DCN^{vGlut2} neurons and their downstream targets during dystonic episodes. (**A**) Schematic of viral strategy and experimental setup for fiber photometry recording in DCN glutamatergic neurons. FN, fastigial nucleus; IN, interposed nucleus. (**B**) Representative histological image indicating AAV-mediated GCaMP6f expression (green) in DCN glutamatergic neurons. The white column denotes the location of the tip of the implanted fiber. Hoechst, blue. Scale bar, 200 μm. (**C** and **D**) Top: Representative calcium traces of DCN glutamatergic neurons in *Prrt2*-mutant;*vGlut2-cre* (C) and wild-type;*vGlut2-cre* (D) mice. The red signs indicate the electrostimulation in seventh Cb. The dark gray shade marks the duration of dystonia. Scale bars, 20 *z*-score by 100 s. Bottom: Heatmaps visualizing GCaMP6f signals aligned to the initiation of dystonia in *Prrt2*-mutant;*vGlut2-cre* ($n = 14$ trials from three mice) (C) and wild-type;*vGlut2-cre* mice ($n = 14$ trials from four mice) (D). Red lines indicate the time of electrostimulation, and dark gray lines mark the initiation of attack in *Prrt2*-mutant mice (C) and the hypothetic onset time in wild-type mice (D). (**E**) Schematic of fiber photometry setup for calcium signal recording in VL of the thalamus. VL, ventral lateral nucleus; RN, red nucleus; SC, spinal cord; DCN, deep cerebellar nuclei. (**F**) Representative image of coronal slice displaying GCaMP6f expression (green) in the thalamus. Solid white column marks the tip site of the implanted fiber. VPL, ventral posterolateral nucleus. Hoechst, blue. (**G** and **H**) Top: Representative Ca^{2+} traces of the VL thalamic neurons in *Prrt2*-mutant (G) and wild-type (H) mice. Scale bars, 20 *z*-score by 100 s. Bottom: Heatmaps illustrating calcium signals aligned to dystonia initiation in *Prrt2*-mutant mice ($n = 18$ trials from three mice) (G) and wild-type ($n = 18$ trials from three mice) (H).

that cerebellar electrostimulation induced an increase in VL calcium signals (Fig. 2G), which exhibited a more rapid decline after reaching peak amplitude compared to calcium dynamics in DCN glutamatergic neurons (Fig. 2, C and G). In contrast, the same cerebellar electrostimulation did not induce substantial calcium fluctuation in the VL nucleus of wild-type mice, nor did these mice display dystonic movements (Fig. 2H). Notably, during dystonic episodes, the increase in neuronal activity in the VL thalamus of *Prrt2*-mutant mice may be driven by direct inputs from glutamatergic DCN neurons or by indirect inputs from other brain regions that are influenced by disturbed cerebellar outputs.

As an additional control, we recorded neuronal activity in the retrosplenial granular cortex (RSG) of *Prrt2*-mutant mice, a brain region that does not receive direct DCN projections (fig. S5, A and B). We found that RSG neurons did not exhibit a noticeable increase in activity following cerebellar cortex stimulation or during dystonic episodes in *Prrt2*-mutant mice (fig. S5, C and D). Together, these findings indicate that DCN glutamatergic neuronal activity is elevated during episodes of *Prrt2*-associated dystonia.

Increased activation of GABAergic IO-projecting and glycinergic DCN neurons during dystonic episodes

GABAergic neurons represent the second most prominent neuronal population in the DCN, participating in various essential cerebellar efferent pathways (*22*, *23*). Among these, GABAergic neurons concentrated in the interposed and dentate nuclei project densely to the inferior olive (IO) nuclei, forming nucleo-olivary projections that play an important role in motor learning and movement direction (*38*–*42*).

Previous studies have established that efferent projections from the interposed and dentate nuclei of the DCN to the IO nuclei are exclusively GABAergic, while those from the fastigial nucleus are primarily excitatory (*40*, *42*). In this study, the GABAergic nature of the IO-projecting neurons in the dentate nucleus was further confirmed (fig. S6, A and B). To focus on whether GABAergic IO-projecting neurons are affected during episodes of dystonia in *Prrt2*-mutant mice, we detected changes in calcium signals in the interposed and dentate nuclei using fiber photometry. We delivered AAV/Retro-hSyn-Cre into the IO nuclei to enable the expression of Cre recombinase in IO-projecting neurons in the DCN (Fig. 3A). We then injected AAV2/8-hSyn-DIO-GCaMP6f into the contralateral interposed and dentate nuclei to specifically express GCaMP6f in DCN GABAergic IO-projecting neurons under the control of Cre recombinase (Fig. 3, A and B). An optical fiber was also targeted to the DCN injection site to record calcium signals from these neurons (Fig. 3, A and B). In *Prrt2*-mutant mice, after delivering electrical stimulation to the cerebellar cortex (seventh Cb), we observed an increase in calcium signals in DCN GABAergic neurons targeting IO nuclei (Fig. 3C). No substantial elevation of calcium signals was

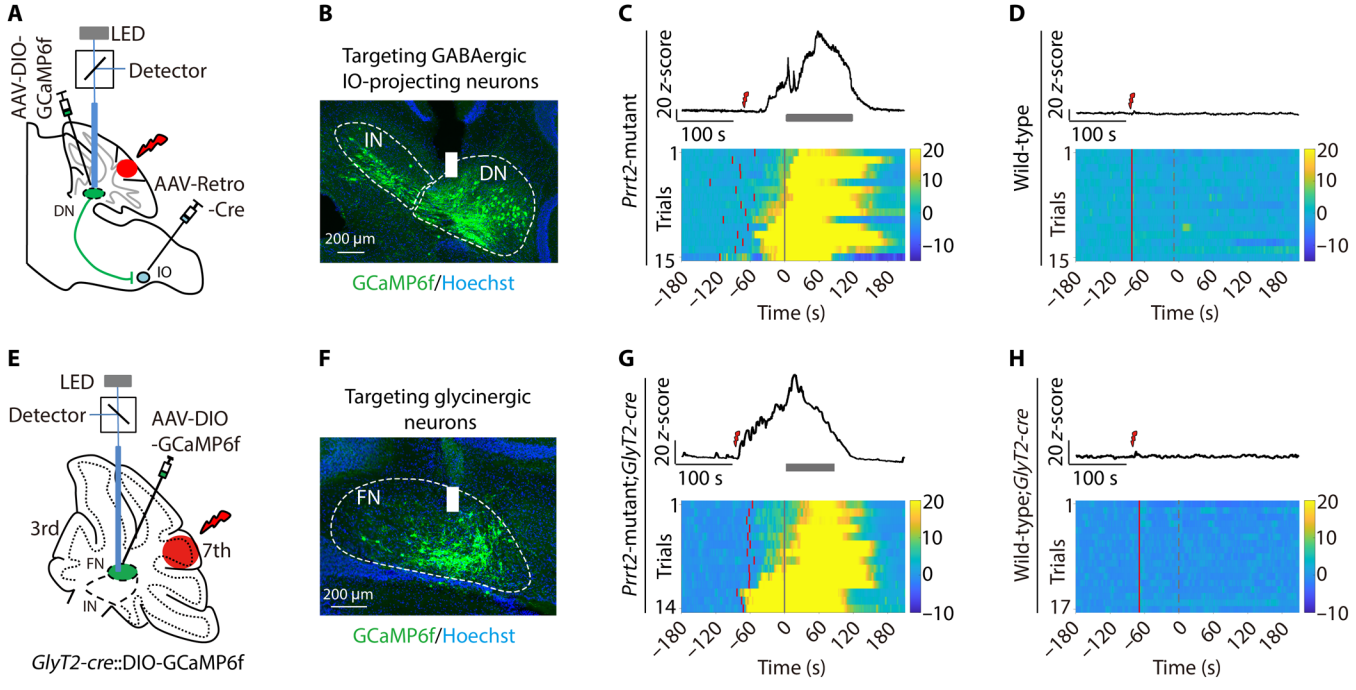

Fig. 3. Increased activation of GABAergic IO-projecting and glycinergic DCN neurons during dystonic episodes. (**A** and **E**) Schematics of viral strategy and experimental setups for fiber photometry recording in GABAergic IO-projecting neurons (A) and glycinergic neurons (E) of the DCN. FN, fastigial nucleus; IN, interposed nucleus; DN, dentate nucleus; IO, inferior olive. (**B** and **F**) Representative images indicating AAV-mediated GCaMP6f expression (green) in GABAergic IO-projecting neurons (B) and glycinergic neurons (F) of the DCN. The dotted lines outline the DCN, and solid white columns mark the tip site of implanted fibers. Hoechst, blue. Scale bars, 200 μm. (**C** and **D**) Top: Representative calcium traces of DCN GABAergic IO-projecting neurons in *Prrt2*-mutant (C) and wild-type (D) mice. The red signs indicate the time of electrostimulation in seventh Cb. Dark gray shade marks the duration of dystonia. Scale bars, 20 *z*-score by 100 s. Bottom: Heatmaps of GCaMP6f signals of DCN GABAergic IO-projecting neurons aligned to the initiation of dystonia in *Prrt2*-mutant ($n = 15$ trials from four mice) (C) and wild-type mice ($n = 15$ trials from four mice) (D). Red lines indicate the time of electrostimulation, and dark gray lines mark the initiation of attack in *Prrt2*-mutant mice (C) and the hypothetic onset time in wild-type mice (D). (**G** and **H**) Top: Representative Ca^{2+} traces of DCN glycinergic neurons in *Prrt2*-mutant;*GlyT2-cre* (G) and wild-type;*GlyT2-cre* (H) mice. Bottom: Heatmaps of GCaMP6f signals aligned to the initiation of dystonia in *Prrt2*-mutant;*GlyT2-cre* ($n = 14$ trials from four mice) (G) and wild-type;*GlyT2-cre* mice ($n = 17$ trials from four mice) (H).

recorded in wild-type mice, which received electrostimulation to the cerebellar cortex and showed no dystonic movements (Fig. 3D).

In addition to glutamatergic and GABAergic neurons, there is a third group of glycinergic neurons in the DCN. Specifically, glycinergic neurons projecting to extracerebellar regions are mainly distributed in the fastigial nucleus (*24*). We applied a similar strategy to assess the responses of these neurons during episodes of dystonia. AAV-hSyn-DIO-GCaMP6f was injected into the fastigial nucleus of the DCN for the selective expression of GCaMP6f in glycinergic neurons in both wild-type (wild-type;*GlyT2-cre*::DIO-GCaMP6f) and *Prrt2*-mutant (*Prrt2*-mutant;*GlyT2-cre*::DIO-GCaMP6f) mice (Fig. 3, E and F). After applying electrostimulation to the cerebellar cortex (seventh Cb), we identified an elevation in the activities of DCN glycinergic neurons in *Prrt2*-mutant mice, but not in wild-type mice (Fig. 3, G and H). Dystonic movements were exclusively observed in *Prrt2*-mutant mice but not in wild-type mice, as mentioned earlier. Collectively, our results showed that three types of DCN neurons examined in this study all experienced sustained activation during episodes of dystonia in *Prrt2*-mutant mice, indicating a widespread activation of DCN neurons during dystonic episodes.

Reduced cerebellar Purkinje cell output to the DCN during episodes of dystonia

The DCN receive massive afferents from a widespread range of brain regions (*29*). The projections from the Purkinje cells in the cerebellar cortex serve as a dominant source of inhibitory inputs in the DCN, connecting with all major groups of DCN neurons (*30*, *31*). A previous study has demonstrated cerebellar SD induced by KCl stimulation suppresses the firing of Purkinje cells (*17*). We have confirmed in this study that electrostimulation can also induce SD in *Prrt2*-mutant mice (fig. S1, A to C). On the basis of these observations, we hypothesized that the inhibitory transmission from Purkinje cells to DCN neurons would be reduced in *Prrt2*-mutant mice suffering from cerebellar SD. This reduction might, in turn, disinhibit several groups of DCN neurons, leading to a sustained increase in activation of DCN neurons in *Prrt2*-mutant mice as aforementioned.

To examine this hypothesis, we recorded calcium signals in the axon terminals of Purkinje cells within DCN. The AAV2/8-PCP2/L7-GCaMP6f virus was used for selective expression of GCaMP6f in Purkinje cells, driven by a minimal PCP2/L7-6 promoter (*43*). To avoid potential contamination from the Purkinje somatic calcium signals, we injected the virus into the fourth and fifth Cbs. These injection sites are anatomically farther from the DCN, thereby reducing the risk of unwanted Purkinje somatic calcium signals being detected by an optical fiber. We targeted the optical fiber to the DCN, where the axon terminals of Purkinje cells project (Fig. 4, A and B). Unexpectedly, after applying electrical stimulation to the seventh Cb, a biphasic change in calcium signals in the axon terminals of Purkinje cells was observed in *Prrt2*-mutant mice (Fig. 4C). By aligning calcium signal data with the initiation of dystonia, we found that the decrease in calcium signals in the axon terminals of Purkinje cells most often occurred during the episodes of dystonia and lasted for about 60 s, while the moderate increase in calcium signals was observed before and after the dystonia attacks in *Prrt2*-mutant mice (Fig. 4C). In

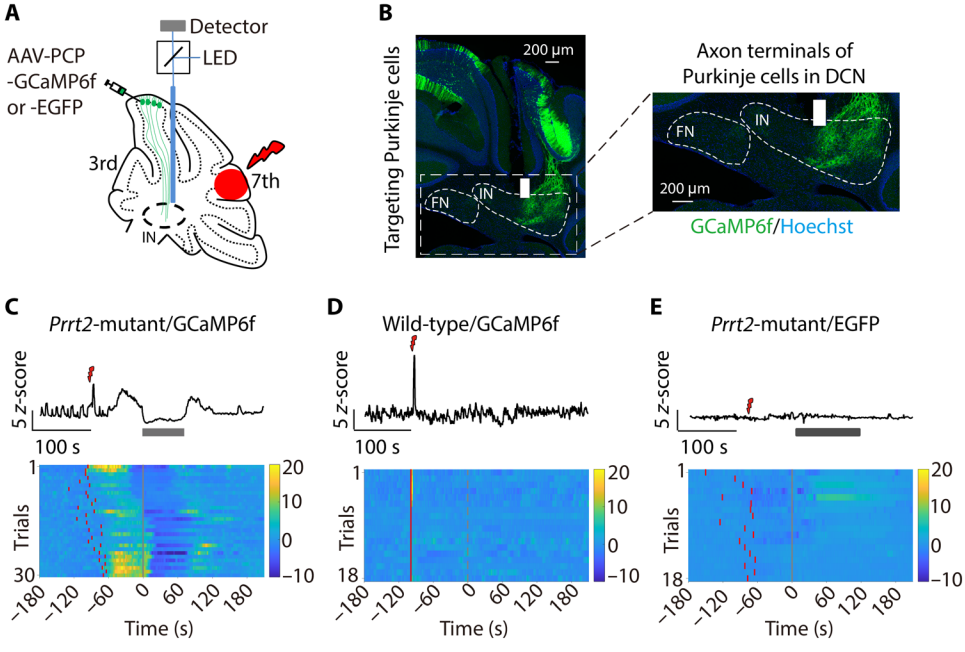

Fig. 4. Reduced cerebellar Purkinje cell output to the DCN during episodes of dystonia. (**A**) Schematic of viral strategy and experimental setup for fiber photometry recording in the axon terminals of Purkinje cells. IN, interposed nucleus. (**B**) Representative images showing GCaMP6f expression (green) in Purkinje cells. The white dashed lines outline the DCN. The white columns mark the tip site of implanted fibers. The areas in the white box are magnified on the right, showing the distribution of GCaMP6f in axon terminals of Purkinje cells within the DCN. Hoechst, blue. Scale bar, 200 μm. (**C** and **D**) Top: Representative calcium traces of the axon terminals of Purkinje cells in *Prrt2*-mutant (C) and wild-type mice (D). The red signs mark the electrostimulation. The dark gray shade indicates the duration of dystonia. Scale bars, 5 *z*-score by 100 s. Bottom: Heatmaps of GCaMP6f fluorescence changes which are aligned to the initiation of dystonia in *Prrt2*-mutant ($n = 30$ trials from five mice) (C) and wild-type mice ($n = 18$ trials from three mice) (D). The red lines indicate the time of electrostimulation. The dark gray lines denote the initiation of attack in *Prrt2*-mutant mice (C) and the hypothetic onset time in wild-type mice (D). (**E**) Top: Representative EGFP trace of the axon terminals of Purkinje cells in *Prrt2*-mutant mice. Scale bar, 5 *z*-score by 100 s. Bottom: Heatmap illustrating EGFP signals aligned to the initiation of dystonia in *Prrt2*-mutant mice ($n = 18$ trials from three mice).

wild-type mice, stimulation of the cerebellar cortex did not elicit a comparable biphasic change in calcium signals nor dystonic movements (Fig. 4D). Furthermore, in an additional control group with enhanced green fluorescent protein (EGFP) expressed at the axon terminals of Purkinje cells in *Prrt2*-mutant mice, we observed no comparable pattern of reduction in fluorescent signals during periods of dystonia (Fig. 4E). In contrast, a slight decrease was detected immediately after cerebellar stimulation (Fig. 4E), likely resulting from the pH changes in Purkinje cells undergoing SD (*44*, *45*). These findings help eliminate the possibility that motion artifacts account for the reduction in calcium signals in the axon terminals of Purkinje cells observed during dystonic movements.

Given that SD-induced suppression of Purkinje cells leads to aberrant activity in DCN neurons, which is involved in dystonic movements of *Prrt2*-mutant mice, we sought to determine whether direct, large-scale suppression of Purkinje cells in wild-type mice could similarly induce dystonia-like behaviors. To achieve widespread Purkinje cell suppression, we injected AAV2/9–PCP2/L7–soma-targeted *Guillardia theta* anion–conducting channelrhodopsin 2 (stGtACR2)–mCherry particles into the fourth to eighth Cbs of wild-type mice. A glass window was placed over the sixth to eighth lobules, and a wide-field light source was used to engage a large cerebellar region (fig. S7, A and B). Upon continuous blue light illumination, all stGtACR2-expressing mice exhibited dystonia-like behaviors during optogenetic inhibition (fig. S7, C and D), whereas control EGFP-expressing mice maintained normal behavior under identical conditions (fig. S7, C and D). Together, these results suggest that the disinhibition resulting from suppression of Purkinje cells inhibitory output may contribute to the widespread increase in DCN neuronal activity observed during dystonic episodes.

Optogenetic stimulation of DCN glutamatergic neurons inducing dystonia-like movements

The observation that three groups of DCN neurons in *Prrt2*-mutant mice exhibit increased activity during dystonic movements raises the question of whether the heightened activity of each group of DCN neurons contributes to dystonia attacks. Here, we combined selective optogenetic stimulation with behavioral assessments to address this issue in freely moving wild-type mice. We opted to use wild-type mice for these experiments to ensure that the motor control system was unaffected by the PRRT2 deficiency, thereby providing a more straightforward context for evaluating the direct behavioral consequences of light stimulation of each neuronal population in the DCN.

We first investigated whether optogenetic activation of DCN glutamatergic neurons could induce dystonic movements. To selectively target the DCN glutamatergic neurons, we injected an AAV virus containing the elongation factor 1α promoter (EF1α)–DIO–channelrhodopsin 2 (ChR2)–mCherry construct into the IN of the DCN in *vGlut2-cre* mice and implanted an optical fiber above the injection site (Fig. 5, A and B). Upon the delivery of continuous or 30-Hz pulsed blue light (470 nm, 4 mW, 20 s) into the DCN, all *vGlut2-cre* animals expressing ChR2-mCherry in DCN glutamatergic neurons (DCN^{vGlut2}-ChR2-mCherry) immediately exhibited dystonia-like postures, characterized by prolonged elevation of limbs (Fig. 5, C and D; fig. S8, A to C; and movie S2). In contrast, control mice expressing EGFP in DCN glutamatergic neurons (DCN^{vGlut2}-EGFP) did not exhibit dystonia-like behaviors when identical blue light stimulation was delivered (fig. S8, D to F). As an additional control, wild-type mice were injected with the AAV-hSyn-ChR2-mCherry virus into the RSG (fig. S9, A and B). These mice showed no dystonia-like behaviors during either continuous or pulsed optogenetic stimulation (fig. S9, C and D).

Subsequently, we explored whether dystonic movements could be triggered by optogenetic activation of GABAergic IO-projecting neurons within the DCN. To selectively express ChR2 in these neurons, we injected AAV-EF1α-DIO-ChR2-mCherry virus into one side of the interposed and dentate nuclei of the DCN in wild-type mice and injected AAV/Retro-hSyn-Cre virus into the contralateral IO nuclei of the same animals (Fig. 5, E and F). Intriguingly, mice expressing ChR2-mCherry in DCN GABAergic IO-projecting neurons ($DCN^{IO\text{-}projecting}$-ChR2-mCherry) did not exhibit dystonia-like behaviors upon continuous or 30-Hz pulsed blue-light stimulation (Fig. 5, G and H; fig. S10, A to C; and movie S3), similar to the observation in the control mice ($DCN^{IO\text{-}projecting}$-EGFP) receiving identical light stimulation (fig. S10, D to F).

Last, we examined whether optogenetic stimulation of DCN glycinergic neurons could induce dystonic movements. We injected AAV-EF1α-DIO-ChR2-mCherry virus into the fastigial nucleus of the DCN in *GlyT2-cre* mice to allow selective expression of ChR2-mCherry in DCN glycinergic neurons (Fig. 5, I and J). When continuous or 30-Hz pulsed blue-light stimulation was delivered to the fastigial nucleus, mice expressing ChR2-mCherry in DCN glycinergic neurons (DCN^{GlyT2}-ChR2-mCherry) exhibited a brief loss of balance at stimulation onset but immediately recovered without displaying any further dystonia-like postures during the stimulation (Fig. 5, K and L; fig. S11, A to C; and movie S4). We did not classify this instantaneous fall as a dystonia-like behavior as it did not meet the criterion, requiring abnormal postures to persist for at least 2 s during stimulation (see Materials and Methods). In the control group (DCN^{GlyT2}-EGFP), the mice displayed no abnormal movements or postures during identical blue-light stimulation (fig. S11, D to F). Together, these findings suggest that the activation of DCN glutamatergic neurons, rather than GABAergic IO-projecting neurons or glycinergic neurons, is primarily responsible for the generation of dystonia-like behaviors in mice.

Ablation of DCN glutamatergic neurons mitigating dystonic movements in mice

Our results have indicated that aberrant activation of DCN glutamatergic neurons is involved in the genesis of dystonic movements (Figs. 2, A to D, and 5, A to D). To further investigate whether the disturbed activity in these glutamatergic neurons is crucial for the manifestation of dystonic movements, we selectively ablated DCN glutamatergic neurons in *Prrt2*-mutant mice (*Prrt2*-mutant;*vGlut2-cre*) by injecting the taCaspase 3 (taCasp3)–encoding AAV particles into bilateral DCN sites, including the fastigial, interposed, and dentate nuclei (Fig. 6A). The co-expression of pro-taCasp3 and tobacco etch virus protease (TEVp) was Cre-dependent, and, once the pro-taCasp3 was proteolyzed by TEVp in cells, taCasp3 effectively induced neuronal apoptosis (*46*). Three weeks after virus injection, we observed a substantial reduction (~98%) in DCN glutamatergic neuron counts in the Casp3 group compared to the mCherry group (Fig. 6, B and C). Ablation of DCN glutamatergic neurons did not impair locomotor activity (fig. S12, A to D), although it did lead to mild ataxia and impaired motor coordination, reflected by slightly reduced performance on rotarod tests and decreased performance on the beam walking tests (fig. S12, E and F). These mild motor

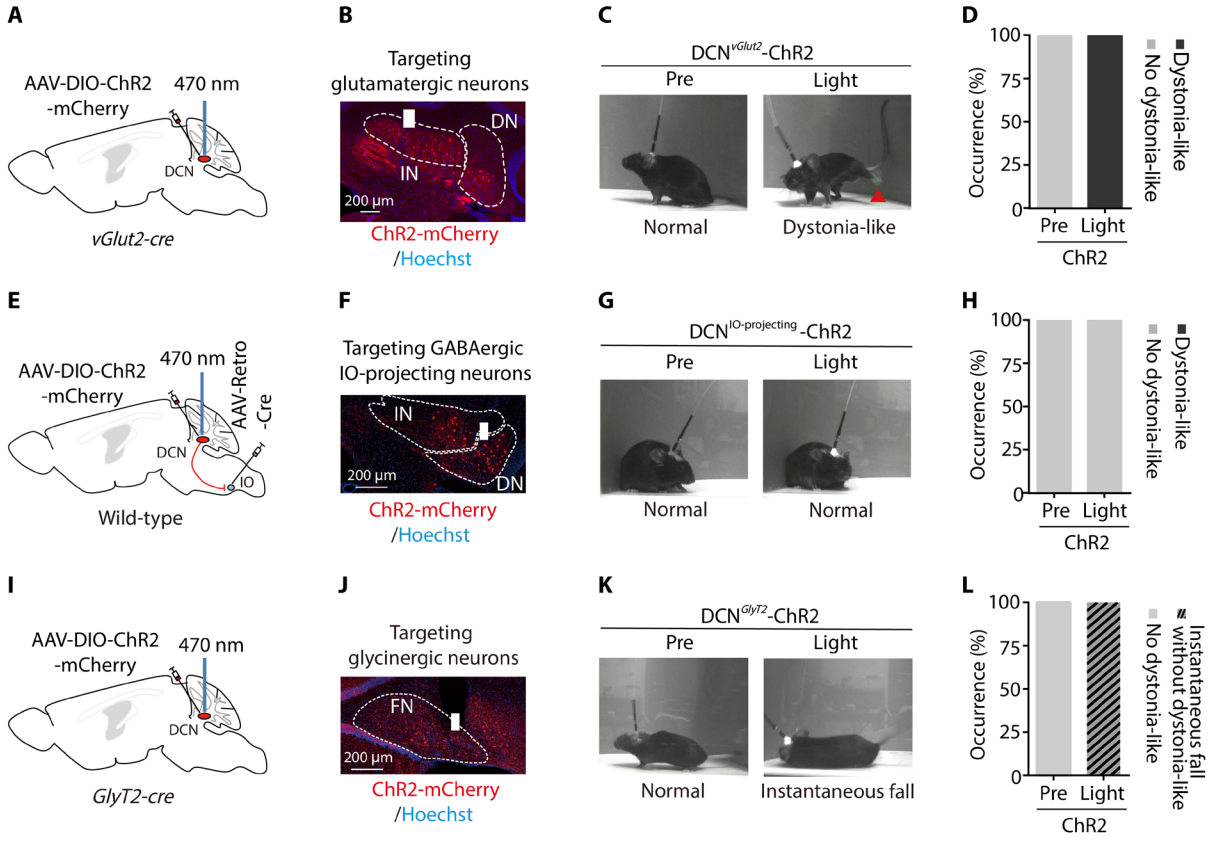

Fig. 5. Optogenetic stimulation of DCN glutamatergic neurons inducing dystonia-like movements. (**A** and **B**) Diagrams of viral strategy (A) and representative histological image of coronal slice depicting the expression of ChR2-mCherry (red) in DCN glutamatergic neurons (B). Dotted lines delineate the DCN outlines, and solid white column denotes the location of implanted fiber. Hoechst, blue. IN, interposed nucleus; DN, dentate nucleus. Scale bar, 200 μm. (**C**) Representative postures of ChR2-expressing *vGlut2-cre* mice before and during light activation. Red arrowhead indicates dystonic movements or postures, like the stiff limbs. (**D**) Percentage of *vGlut2-cre* mice ($n = 4$ mice) displaying dystonia-like behaviors. (**E** and **F**) Diagrams of viral strategy (E) and representative histological image of the expression of ChR2-mCherry (red) in DCN GABAergic IO-projecting neurons (F). Scale bar, 200 μm. (**G**) Representative postures of mice before and during light activation on DCN GABAergic IO-projecting neurons. (**H**) Percentage of wild-type mice ($n = 4$ mice) exhibiting dystonia-like behaviors before and during light stimulation. (**I** and **J**) Diagrams of viral strategy (I) and representative histological image of the expression of ChR2-mCherry (red) in DCN glycinergic neurons (J). FN, fastigial nucleus. Scale bar, 200 μm. (**K**) Representative postures of ChR2-expressing *GlyT2-cre* mice before and during light activation. (**L**) Percentage of occurrence of dystonia-like behaviors or instantaneous fall without dystonia-like behaviors in *GlyT2-cre* mice ($n = 4$ mice) before and during light stimulation.

deficits following DCN glutamatergic neuron ablation align with previous findings (*47*), possibly due to compensatory functional adaptations within the brain (*48*).

Upon delivering electrical stimulation to the cerebellar cortex (seventh Cb) of *Prrt2*-mutant mice with DCN glutamatergic neuron ablation (*Prrt2*-mutant;*vGlut2-cre*::DIO-Casp3), we observed minimal dystonic movements in these mice (Fig. 6, D and E, and movie S5). In contrast, mCherry-expressing *Prrt2*-mutant mice (*Prrt2*-mutant;*vGlut2-cre*::DIO-mCherry) with intact glutamatergic DCN neurons exhibited severe dystonia attacks in response to identical cerebellar electrostimulation (Fig. 6, D and E, and movie S5), consistent with our aforementioned observations.

In an additional experiment, we evaluated the effects of glutamatergic DCN neuron ablation on neuronal responses within the VL thalamus, one of the targets of DCN glutamatergic neurons, in *Prrt2*-mutant mice (Fig. 6F). We observed that electrical stimulation of the cerebellar cortex (seventh Cb) neither evoked a pronounced calcium signal increase in the VL thalamus nor induced severe dystonia in *Prrt2*-mutant mice with glutamatergic DCN neuron ablation (Fig. 6G). This contrasts with the observations in the mCherry-expressing *Prrt2*-mutant mice, which were subjected to identical cerebellar electrostimulation and displayed dystonic movements accompanied by elevated calcium signals in the VL thalamus (Fig. 6H).

Additionally, we further examine the roles of GABAergic IO-projecting and glycinergic DCN neurons in *Prrt2*-associated dystonia by ablating these neuronal populations, respectively, in *Prrt2*-mutant mice using a Casp3-mediated ablation strategy. Specifically, to ablate GABAergic IO-projecting neurons, we injected the Cre-dependent taCasp3-encoding AAV particles into the dentate nucleus of DCN in *Prrt2*-mutant mice, along with an AAV/Retro-Cre virus into the IO nuclei of the same animals (fig. S13, A to E). For DCN glycinergic neuron ablation, we delivered the same AAV-DIO-Casp3 virus into the fastigial nucleus of *Prrt2*-mutant mice (*Prrt2*-mutant;*GlyT2-cre*::DIO-Casp3) (fig. S13, F to J). Neither of these specific ablations reduced dystonia severity following cerebellar electrostimulation in *Prrt2*-mutant mice (fig. S13, D to E and I to J). These findings reinforce the notion that DCN glutamatergic neurons, rather than glycinergic or GABAergic IO-projecting neurons, mediate dystonic

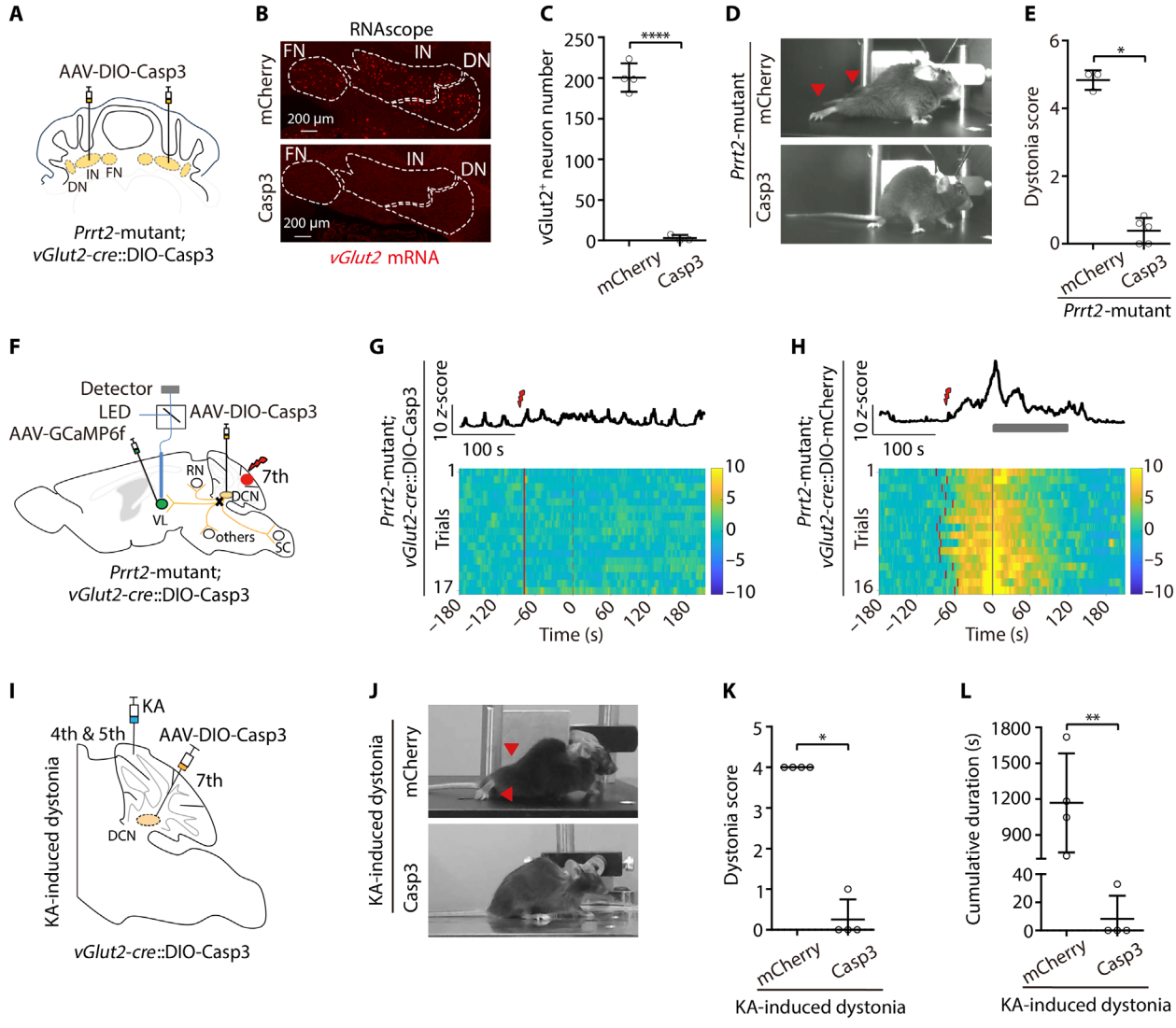

Fig. 6. Ablation of DCN glutamatergic neurons mitigating dystonic movements in mice. (**A**) Illustration showing targeted ablation of DCN glutamatergic neurons in *Prrt2*-mutant mice. (**B**) Representative images showing *vGlut2* mRNA signals in the DCN. Scale bars, 200 μm. (**C**) Quantification of numbers of glutamatergic neurons in the DCN of mCherry mice ($n = 4$ mice) and Casp3 mice ($n = 3$ mice). $^{****}P < 0.0001$, Unpaired Student's t test. (**D**) Representative postures in mice following electrostimulation. Red arrowheads mark dystonic postures. (**E**) Dystonia score comparison between mCherry/*Prrt2*-mutant ($n = 3$ mice) and Casp3/*Prrt2*-mutant mice ($n = 5$ mice). $^{*}P < 0.05$, Mann-Whitney U test. (**F**) Schematic diagram for viral strategy and fiber photometry recording in the VL thalamus. (**G** and **H**) Top: Representative traces showing changes in GCaMP6f fluorescence. Gray shade marks the duration of dystonia. Scale bars, 10 z-score by 100 s. Bottom: Heatmaps illustrating the calcium response of VL neurons in Casp3/*Prrt2*-mutant mice ($n = 17$ trials from three mice) (G) and mCherry/*Prrt2*-mutant mice ($n = 16$ trials from three mice) (H). The red lines mark the time of electrostimulation. The gray lines denote the hypothetic attack onset time in Casp3/*Prrt2*-mutant mice (G) and the initiation of attack in mCherry/*Prrt2*-mutant mice (H). (**I**) Schematic illustrating the viral strategy and KA microinjection in *vGlut2-cre* mice. KA, kainic acid. (**J**) Representative postures in mice following KA microinjection. (**K**) Quantification of dystonia score in mCherry ($n = 4$ mice) and Casp3 mice ($n = 4$ mice). $^{*}P < 0.05$, Mann-Whitney U test. (**L**) The cumulative duration of dystonia attacks in mCherry ($n = 4$ mice) and Casp3 mice ($n = 4$ mice) during the period (40 to 70 min post-KA microinjection). $^{**}P < 0.01$, Unpaired Student's t test. (C, E, K, and L) Data were represented as means ± SEM.

movements triggered by cerebellar electrical stimulation in *Prrt2*-mutant mice.

To expand on our findings, we investigated the role of DCN glutamatergic neurons in a classical model of cerebellar-originated dystonia, induced by localized kainic acid injection into the cerebellar cortex of wild-type mice (*14*). Unlike the dystonic movements observed in *Prrt2*-mutant mice following cerebellar electrostimulation, kainic acid–treated mice exhibited recurrent dystonia attacks of exceptionally prolonged duration (lasting more than 2 hours), consistent with previous observations (*14*). dc-ECoG recording from the cerebellar cortex revealed two distinct stages following kainic acid injection (fig. S14, A and B). In the early stage, repetitive dystonic movements occurred without detectable SD events, reflected by the absence of dc-shift signals. However, in the late stage, dystonic behaviors coincided with SD-like events in the cerebellar cortex (fig. S14, A and B). To investigate glutamatergic DCN neuronal activity during these dystonic episodes, we performed fiber photometry calcium imaging in the IN of *vGlut2-cre* mice (fig. S14, C and D).

Following localized kainic acid injection into the cerebellar cortex, Ca^{2+} levels increased in these neurons during bouts of dystonia in both early and late stages (fig. S14, E and F). These findings further confirm the close association between the aberrant activity of glutamatergic DCN neurons and dystonic behaviors.

Last, to directly examine the role of glutamatergic DCN neurons in kainic acid–induced dystonia, we selectively ablated these neurons using the aforementioned strategy (Fig. 6I). Three weeks post-ablation, kainic acid was delivered to the fourth and fifth Cbs of mice (Fig. 6I), followed by comparative analyses of dystonic behaviors. We found that *vGlut2-cre* mice with DCN glutamatergic neuron ablation displayed reduced dystonia attacks compared to those in the mCherry group (*vGlut2-cre*::DIO-mCherry) (Fig. 6, J to L, and movie S6). This reduction was characterized by a substantial decrease in both the severity and cumulative duration of dystonic behaviors (Fig. 6, K and L), echoing results obtained in *Prrt2*-mutant mice with the deletion of glutamatergic neurons in the DCN. Together, these findings provide compelling evidence that DCN glutamatergic neurons are essential for dystonic movement expression, and their disrupted activity mediates cerebellar-originated dystonia.

DISCUSSION

The DCN play a pivotal role in cerebellar functions and have been implicated in the pathophysiology of dystonia. Previous studies using in vivo extracellular recordings delineated irregular firing patterns of DCN neurons in various mouse models of dystonia (*9*, *10*, *12*). However, these methods lacked the resolution to differentiate the contributions of specific neuronal populations in dystonia. In this study, through fiber photometry recordings, cell-type–specific optogenetic manipulations, and targeted neuronal ablations, we highlight the critical role of glutamatergic DCN neurons in mediating dystonic movements in *Prrt2*-mutant mice. This role of glutamatergic DCN neurons is likely crucial not only in *Prrt2*-associated dystonia but also in other cerebellar-originated dystonic conditions, such as kainic acid–induced dystonia models.

The etiology of dystonia is multifaceted, encompassing inherited mutations in genes, such as mutations in *TOR1A*, *ATP1A3*, *GANL*, *IP3R1*, *CACAN1A*, and *PRRT2* (*49*–*54*), as well as acquired factors including infections, drugs and brain injuries (*1*). Researchers have used various genetically engineered and chemical-induced animal models to investigate mechanisms of dystonia (*55*). These studies have revealed that multiple motor-associated brain regions were involved in dystonic movements, including the cerebellum, motor cortex, basal ganglia, thalamus, spinal cord, and interconnected neural circuits (*10*, *14*, *16*–*18*, *56*–*60*).

Previous studies indicated that enhanced cerebellar susceptibility to SD underlies *Prrt2*-associated dystonia (*17*). PRRT2 acts as a regulator of voltage-dependent sodium channels (Nav channels), modulating neuronal excitability by reducing the availability of functional Nav channels (*17*, *61*, *62*). Loss of PRRT2 increases excitability in cerebellar granule cells, facilitating cerebellar SD in *Prrt2*-mutant mice (*17*). In *Prrt2*-mutant mice, the onset of dystonia was notably delayed relative to the elevation of calcium signals in the DCN induced by localized cerebellar stimulation. This phenomenon is likely attributed to slow SD propagation and cerebellar circuit organization.

When the SD was initiated by localized cerebellar stimulation in *Prrt2*-mutant mice, it propagates slowly through the cerebellar cortex at ~1.6 mm/min (*17*). Initially, only a limited portion of the cerebellar cortex was affected by the SD, exerting a moderate influence on DCN neurons that was insufficient to trigger dystonic behaviors. As SD expanded, it progressively engaged a larger extent of the cerebellar cortex, likely involving critical motor-associated regions, such as the anterior Cbs (*63*). Once accumulated aberrant inputs exceeded a critical threshold, the activity of glutamatergic DCN neurons became sufficiently disrupted, triggering dystonic behaviors through downstream premotor circuits. This progressive recruitment process within the DCN might account for the relatively long latency of dystonia observed in *Prrt2*-mutant mice.

In contrast, direct optogenetic stimulation of glutamatergic DCN neurons in wild-type mice mimicked the abrupt calcium activity increase observed during dystonic episodes in *Prrt2*-mutant mice, bypassing the slower upstream processes in cerebellar cortex, and resulted in immediate dystonia-like behaviors during stimulation. The direct activation experiments support the hypothesis that DCN glutamatergic neurons critically mediate dystonic behaviors.

DCN neurons exhibit spontaneous firing, and their activity is modulated by various inputs, including inhibitory inputs from Purkinje cells and excitatory inputs from mossy fibers (*29*–*31*). Our findings revealed a two-phase increase in calcium signals in DCN glutamatergic neurons, characterized by an initial mild elevation followed by an abrupt rise in intracellular Ca^{2+} levels. The moderate calcium elevation in DCN neurons occurred shortly after cerebellar stimulation and preceded the onset of dystonic episodes in *Prrt2*-mutant mice. Notably, a simultaneous increase in calcium signals was also observed in the axon terminals of Purkinje cells. This concurrent activation of Purkinje cells and DCN neurons appears paradoxical, given their inhibitory relationship. We propose that cerebellar stimulation initially activates precerebellar systems, possibly through a feedforward mechanism, resulting in the simultaneous excitation of both Purkinje cells and DCN neurons via excitatory mossy fiber inputs.

Subsequently, as SD progressively affected a greater number of Purkinje cells arranged across multiple Cbs (*64*, *65*) and drove them into a depressed state, their tonic inhibition inputs to DCN neurons were diminished. This disinhibition led to a rapid and pronounced increase in DCN neuronal activity, which was then followed by depolarization block (*17*). At the level of individual DCN neurons, this sequence of initial hyperactivity followed by depolarization block reflects severe firing irregularities during dystonic episodes, aligning with findings from previous studies (*9*, *10*, *12*). It is worth noting that, during depolarization block, neurons are unable to effectively generate action potentials despite maintaining elevated intracellular calcium levels (*62*). This may explain the discrepancy between electrophysiological recordings of firing activity (*17*) and calcium signal dynamics in the DCN during dystonic episodes in *Prrt2*-mutant mice.

Glutamatergic neurons within the DCN project widely to the thalamus, red nucleus, spinal cord, and brainstem targets (*23*). Several thalamic nuclei, including the ventral lateral, ventral medial, centrolateral (CL), and parafascicular nuclei, receive excitatory DCN projections via the ascending pathway (*23*, *66*). Previous studies have implicated the DCN-CL thalamus pathway in animal models of ouabain-induced dystonia and DYT25 dystonia (*11*, *58*), although the contributions of other thalamic nuclei to dystonia remain unclear. Given that the projections from the DCN to the CL thalamus are excitatory (*35*, *67*), it is postulated that glutamatergic neurons in the DCN contribute to the animal model of cerebellar-induced dystonia.

Notably, excitatory DCN neurons project with collateralization across multiple motor-related extracerebellar regions (*23*, *27*, *37*). This projection pattern suggests that stimulation of DCN glutamatergic neurons may concurrently activate multiple downstream circuits through both ascending and descending pathways, thereby inducing dystonic behaviors. This hypothesis aligns with the motor network disorder theory of dystonia (*68*–*70*).

Glycinergic neurons within the DCN primarily project to the cerebellar cortex and ipsilateral brainstem regions, specifically the vestibular nuclei (VN) and the medullary reticular formation (MedRF) (*24*, *71*). The VN are renowned for their involvement in tasks such as maintaining balance, spatial orientation, and gaze stabilization (*72*, *73*), while the MedRF typically orchestrates functions related to head movements and gaze holding (*74*). Our study revealed that activation of DCN glycinergic neurons in mice led to a momentary loss of balance rather than lasting dystonia-like behaviors. It is plausible that activation of glycinergic VN-projecting neurons in the DCN causes the instantaneous fall in the mice. Overall, on the basis of the evidence from the experiments of optogenetic stimulation and ablation of glycinergic neurons, we suggested that glycinergic neurons in the fastigial nucleus play a minor role in the generation of dystonia.

In the DCN, a group of GABAergic neurons is primarily located in the interposed and dentate nuclei, projecting to the IO nuclei in the medulla oblongata (*39*). Recent studies have reported that genetic elimination of the transmission from the IO to Purkinje cells leads to reliable and nonreversible dystonic behavior in $Ptf1a^{Cre/+}$;$Vglut2^{flox/flox}$ mice (*12*). In this study, we hypothesized that stimulating GABAergic IO-projecting neurons in the DCN would enhance inhibitory transmission in the IO nuclei, thereby reducing the excitatory outputs of IO neurons to Purkinje cells and disturbing mouse movements. Unexpectedly, dystonia-like behavior was absent during the activation of DCN GABAergic IO-projecting neurons. This outcome suggests that the activation of these DCN neurons may not sufficiently disturb the activity of enough IO neurons to induce dystonic movements, as reported in mice entirely lacking fast glutamatergic neurotransmission in climbing fibers (*12*). In addition, recent studies have shown that the IO nuclei receives both excitatory and inhibitory projections from the fastigial and dentate nuclei, respectively (*40*). Our study did not separately explore the excitatory IO-projecting DCN neurons, and, while our findings suggest that GABAergic IO-projecting neurons in the dentate nucleus play a limited role in generating dystonia-like behaviors compared to the DCN glutamatergic neurons, they do not exclude the potential involvement of the nucleo-olivary pathway in dystonic behaviors.

In addition to GABAergic IO-projecting neurons, the DCN also contain a substantial population of local GABAergic interneurons, as well as GABAergic projection neurons that target nuclei associated with motor and sensory functions (*22*, *23*). Recent work identified five inhibitory cell types within the DCN, distinguished by specific expression of characterized genes (*21*). However, at present, we still lack the available tools to selectively target these distinctive groups of GABAergic neurons in the DCN. Further investigation is warranted to understand the roles of various GABAergic neuronal subpopulations in the DCN and their contributions to dystonia.

Abnormal outputs from the DCN have been considered a potent target for the treatment of dystonia (*7*, *11*, *12*, *16*–*20*). Several strategies have been developed to modulate the dysregulated DCN outputs in dystonic animals. For example, cerebellar nucleus lesion or cerebellectomy demonstrated efficacy in diminishing dystonic movements in genetically dystonic rats (*19*, *20*). The disconnection of the link between the DCN and basal ganglia proved to be effective in alleviating dystonia in ouabain-treated mice (*11*). Silencing of the DCN using osmotically delivered lidocaine effectively eliminated dystonia-associated tremors in $Ptf1a^{Cre/+}$;$Vglut2^{flox/flox}$ mice (*12*). Additionally, systematic treatments with anti-convulsant drugs, such as carbamazepine or lacosamide, exhibited benefits in relieving *Prrt2*-associated dystonia, which was associated with aberrant activities in the DCN (*17*). Most recently, DBS has shown promising results in animal models of dystonia. Targeting the DBS specifically to the DCN of $Ptf1a^{Cre/+}$;$Vglut2^{flox/flox}$ mice resulted in remarkable immediate improvements in dystonic behaviors (*7*, *12*). In this study, we confirmed that ablation of DCN glutamatergic neurons could potentially ameliorate dystonic movements in both the *Prrt2*-associated dystonia model and the kainic acid–induced dystonia model. This finding indicates the pivotal involvement of DCN glutamatergic neurons in the dystonia across different etiologies. In addition to the ablation strategy, modulating the activity of DCN glutamatergic neurons to intervene in dystonia attacks is promising (*12*, *75*). However, it remains technically challenging to target and manipulate these neurons specifically and effectively across all three DCN nuclei.

There were several limitations in this study. First, while our results confirm that abnormal outputs from DCN glutamatergic neurons mediate dystonic behaviors, it remains unclear how distinct subpopulations of these neurons, such as those projecting to the thalamus, brainstem, and spinal cord, interact to modulate the dystonic movements. Second, while we proposed sequential changes in activity within the cerebellar circuit based on our observations of calcium signals in axon terminals of Purkinje cells and DCN neurons, the propagation characteristics of cerebellar SD, coupled with the inherent temporal limitations of fiber photometry, make it challenging to accurately determine the precise sequence of neuronal activity changes across these nodes. Third, in this study, we focused on the role of DCN neuronal groups projecting outside the cerebellum in dystonia. However, there are several subgroups of DCN neurons sending projections to the cerebellar cortex, forming nucleo-cortical pathways (*26*, *71*, *76*). These DCN neurons, such as DCN glycinergic cells projecting to the granule cell layer of the cerebellar cortex and forming synaptic connections with Golgi cells (*71*), were not selectively explored in this study. Collectively, our findings delineate the pivotal role of DCN glutamatergic neurons in the pathogenesis of dystonia and may guide the development of targeted therapies for cerebellar-originated dystonia.

MATERIALS AND METHODS

Experimental design

In this study, we devised a series of experiments to elucidate the role of three distinct populations of neurons within the DCN in dystonia. The *Prrt2*-mutant mice and a kainic acid–induced dystonia animal model were used in this study. First, we used cell-type–specific targeting and calcium signal recording techniques to monitor the activity of three neuronal populations in DCN during episodes of dystonia in *Prrt2*-mutant mice. Then, optogenetic manipulations were used to determine whether the activity of three types of DCN neurons contributed to dystonia attacks. Last, we used a selective ablation strategy to probe whether the aberrant outputs from DCN

glutamatergic neurons were necessary for the dystonia attacks in *Prrt2*-associated and kainic acid–induced dystonia animal models.

Animals

C57BL/6J mice were purchased from the Shanghai Laboratory Animal Research Center. *vGlut2-cre* (JAX: 016963) mice were obtained from the Jackson Laboratory. *GlyT2-cre* (RBRC: 10109) mice were acquired from RIKEN BRC.

In this study, *Prrt2*-mutant mice harboring premature stop codon in exon 2 of the proline-rich transmembrane protein 2 (*Prrt2*) gene were used (*28*). These mice were bred for more than 10 generations on a C57BL/6J background. To specifically monitor calcium signals in distinct neuronal populations in the DCN, *Prrt2*-mutant;*vGlut2-cre* mice and *Prrt2*-mutant;*GlyT2-cre* mice were generated by crossing *Prrt2*-mutant mice with two Cre-driver mouse lines, respectively: *vGlut2-cre* mice and *GlyT2-cre* mice. In these lines, *Prrt2* mutation resulted in the loss of PRRT2 protein expression in the mouse brain, while Cre recombinase was specifically expressed in glutamatergic and glycinergic neurons, respectively.

Mice were subjected to a 12-hour light/dark cycle (light on at 7:00 a.m.) with ad libitum food and water. All experimental procedures conducted in this study were approved by the Animal Care and Use Committee of the Center for Excellence in Brain Science and Intelligence Technology, Chinese Academy of Sciences, Shanghai, China (approval number, NA-009-2022). Both male and female animals aged 8 to 16 weeks were used in this study.

Viruses

In this study, the following viral tools were applied: AAV2/9-hSyn-GCaMP6f-WPRE-pA (2.22×10^{13} vector genomes (v.g.)/ml; Shanghai Taitool Bioscience, no. S0536-9-H20), AAV2/8-hSyn-DIO-GCaMP6f-WPRE-pA (4×10^{13} v.g./ml; Institute of Neuroscience Gene Editing Core, no. GP80), AAV2/8-PCP2/L7-GCaMP6f-WPRE-pA (1.47×10^{13} v.g./ml; Shanghai Taitool Bioscience, no. S0664-8), AAV2/9-PCP2/L7-stGtACR2-mCherry-WPRE-pA (1.73×10^{13} v.g./ml; Shanghai Taitool Bioscience, no. S1393-9-H20), AAV2/8-PCP2/L7-EGFP-WPRE-pA (1.31×10^{13} v.g./ml; Shanghai Taitool Bioscience, no. WY3091), AAV2/9-hEF1α-DIO-EGFP-WPRE-pA (1.14×10^{13} v.g./ml; Shanghai Taitool Bioscience, no. S0270-9-H20), AAV2/9-EF1α-DIO-hChR2(H134R)-mCherry-WPRE-pA (1.15×10^{13} v.g./ml; Institute of Neuroscience Gene Editing Core, no. 20297), AAV2/9-hSyn-hChR2(H134R)-mCherry-WPRE-pA (1.28×10^{13} v.g./ml; Shanghai Taitool Bioscience, no. S0165-9-H20), AAV2/9-CAG-DIO-taCaspase3-TEVp-WPRE-pA (1.08×10^{13} v.g./ml; Shanghai Taitool Bioscience, no. S0236-9-H20), scAAV2/2Retro-hSyn-Cre-pA (1.65×10^{13} v.g./ml; Shanghai Taitool Bioscience, no. S0292-2R-H20), and AAV2/8-EF1α-DIO-mCherry-WPRE-pA (1.43×10^{13} v.g./ml; Institute of Neuroscience Gene Editing Core, no. 50462). Viruses were aliquoted and stored at −80°C until use.

Surgery

Mice administered meloxicam (5 mg/kg, subcutaneously) 30 min before surgery for intraoperative analgesia. Mice were anesthetized with isoflurane (4% for induction and 2% for maintenance) and placed on a stereotaxic frame (David Kopf Instrument, Model 942). Body temperature was maintained using a heating pad throughout the surgery. To keep the eyes moist, erythromycin eye ointment (Front Pharmaceutical Co. Ltd) was applied. For perioperative analgesia, mice received 2% lidocaine injections at incision sites every 30 min during the surgery. After that, a midline incision was made to expose the skull, and 2% hydrogen peroxide was used to clean the connective tissue on the skull surface. A custom-made head plate was attached to the skull using light-curing self-etch adhesive (3M ESPE Single Bond Universal) and dental cement. Subsequently, a portion of the skull above the target area was carefully removed with a surgical drill.

For virus and drug injection, a Nanoject III (Drummond Scientific Company) was used to deliver the substance into the target at a speed of 1 nl/s. Each 20 nl of injection was followed by a 15-s pause interval. After the finish of injection, the glass pipette was kept in place for an additional 10 min before being retracted. In the case of chronic implantation, optical fibers and metal electrodes were positioned in the target brain area and secured to the skull using dental cement. Postoperatively, mice received meloxicam (5 mg/kg, subcutaneously) every 24 hours for 3 days for analgesia, and a recovery period of at least 2 weeks was allowed to recuperate and enable AAV-mediated transgene expression.

Electrostimulation

Mice were anesthetized and prepared in accordance with the procedures outlined in the surgery section. Specifically, two small holes spaced 1.5 mm apart were drilled into the skull at the seventh Cb or fourth and fifth Cbs [anterior-posterior (AP), −6.48 mm; medial-lateral (ML), 0 mm; and dorsal-ventral (DV), −1 mm] to facilitate the insertion of two metal electrodes (100 μm in diameter, California Fine Wire). These electrodes were implanted at a depth of −0.45 mm from the dura and secured in place using dental cement.

One week post-surgery, the mouse was affixed to a custom-designed head plate holder. The pre-implanted metal electrodes were connected to a stimulus isolator (AMPI, ISO Flex). The electrical stimulation (200 to 500 μA) was delivered through the isolator, featuring a frequency of 20 Hz and a pulse width of 1 ms, lasting for 2.5 to 5 s.

ECoG recording in the cerebral cortex

To investigate whether the attacks in *Prrt2*-mutant mice are associated with epileptiform activity, ECoG recording was performed in the cerebral cortex. Two metal electrodes (100 μm in diameter, California Fine Wire) were bilaterally implanted in the motor cortex (AP, −0.34 mm; ML, ±1 mm; and DV, −0.6 mm) of *Prrt2*-mutant mice. One week after surgery, the mice were habituated to a head-fixed condition for 1 hour before recording. ECoG signals (1 to 300 Hz) were amplified 100× using an alternating current (ac)/dc differential amplifier (Model 3000, A-M Systems) and digitized at 1 kHz with a Digidata 1332A (Molecular Devices). Recordings lasted 10 min per mouse. Electrical stimuli were applied to the seventh Cb immediately following a 2-min baseline period. Animal behavior was simultaneously recorded using a camera. After a 1-day recovery period, mice received an intraperitoneal injection of pentylenetetrazol (60 mg/kg) to induce tonic-clonic seizures, and ECoG signals were recorded for 30 min.

dc-ECoG recording in cerebellar cortex

To investigate whether SD occurs in the cerebellar cortex of *Prrt2*-associated and KA-induced dystonia animal models, we conducted dc-ECoG recordings in the cerebellar cortex. Recording electrodes (33 μm in diameter, California Fine Wire) were implanted in the fourth and fifth Cbs of mice, with a reference electrode implanted in

the motor cortex. One week after surgery, following a 1-hour head-fixation acclimation, recordings were performed. ECoG signals (dc to 1000 Hz) were amplified 100× with an ac/dc differential amplifier and sampled at 1 kHz through a digitizer.

Ablation of DCN neurons

For the ablation of DCN glutamatergic neurons, 360 nl of AAV particles (AAV2/9-CAG-DIO-taCaspase3-TEVp-WPRE-pA or AAV2/8-EF1α-DIO-mCherry-WPRE-pA) were bilaterally injected into the entire DCN (AP, −6.48 mm; ML, ±0.95 mm; and DV, −2.45 mm; AP, −6.36 mm; ML, ±1.5 mm; and DV, −2.45 mm; and AP, −6 mm, ML, ±2.15 mm; and DV, −2.45 mm) of *Prrt2*-mutant;*vGlut2-cre* and *vGlut2-cre* mice.

For the ablation of DCN glycinergic neurons, 200 nl of AAV particles were bilaterally injected into the fastigial nucleus (AP, −6.48 mm; ML, ±0.95 mm; and DV, −2.45 mm) of *Prrt2*-mutant;*GlyT2-cre* mice. To ablate DCN GABAergic IO-projecting neurons, 300 nl of AAV particles were bilaterally injected into the dentate nucleus (AP, −6 mm; ML, ±2.15 mm; and DV, −2.45 mm), with an additional 200 nl of AAV particles (scAAV2/2Retro-hSyn-Cre-pA) injected into the IO (AP, −6.96 mm; ML, ±0.38 mm; and DV, −5.5 mm) in *Prrt2*-mutant mice.

Kainic acid microinjection

To further explore the potential alleviation of dystonic behaviors through the ablation of glutamatergic neurons in the DCN in other animal models of dystonia, a cerebellar-originated dystonia mouse model induced by injecting kainic acid in the cerebellum was used. The kainic acid monohydrate (Sigma-Aldrich, no. K0250-10MG) used in our study was dissolved in 0.9% sterile saline, with the pH adjusted to 7.4. A 10 mM solution of kainic acid, with a volume of 23.4 nl, was administered to the fourth and fifth Cbs (AP -6.48 mm, ML 0 mm, DV -1 mm) in *vGlut2-cre* mice.

After the injection, the mice were securely fixed on a custom-designed head plate holder. Behavioral observations were systematically conducted and recorded using a camera for at least 2 hours.

Fiber photometry recording in the DCN

In this study, the rationale for targeting specific nuclei in DCN was based on the distribution features of the neuronal populations of interest. To determine the activities of DCN neurons during episodes of dystonia in *Prrt2*-mutant mice, we used fiber photometry to monitor calcium signals in the IN of DCN. AAV2/9-hSyn-GCaMP6f-WPRE-pA virus (200 nl; 2×10^{12} v.g./ml) was unilaterally injected into the DCN (AP, −6.36 mm; ML, 1.5 mm; and DV, −2.45 mm).

To assess alterations in calcium signals within DCN glutamatergic neurons of *Prrt2*-associated and KA-induced dystonia animal models, 200 nl of AAV2/8-hSyn-DIO-GCaMP6f-WPRE-pA virus was injected into either the right IN (AP, −6.36 mm; ML, 1.5 mm; and DV, −2.45 mm) or left fastigial nucleus (AP, −6.48 mm; ML, −0.95 mm; and DV, −2.45 mm) of *Prrt2*-mutant;*vGlut2-cre* and *vGlut2-cre* mice.

For the observation of calcium signals in DCN glycinergic neurons, 200 nl of AAV2/8-hSyn-DIO-GCaMP6f-WPRE-pA virus was injected into the right fastigial nucleus (AP, −6.48 mm; ML, 0.95 mm; and DV, −2.45 mm) of *Prrt2*-mutant;*GlyT2-cre* and *GlyT2-cre* mice.

To record calcium signals in DCN GABAergic IO-projecting neurons, 300 nl of AAV2/8-hSyn-DIO-GCaMP6f-WPRE-pA virus was injected into the right interposed and dentate nuclei (AP, −6 mm; ML, 2.15 mm; and DV, −2.45 mm), and 200 nl of scAAV2/2Retro-hSyn-Cre-pA virus was injected into the left IO nuclei (AP, −6.96 mm; ML, −0.38 mm; and DV, −5.5 mm) of *Prrt2*-mutant and wild-type mice.

Subsequently, fiber-optic cannulas (Shanghai June Bio Tech, no. LC20040na0.37P) were implanted with the end of the optical fiber targeted to 0.15 mm above the injection sites of the DCN. Two metal electrodes were implanted in the seventh Cb of the animals 1 week later. Fiber photometry recordings were performed 3 weeks after virus injection to ensure sufficient viral expression.

During fiber photometry recordings, animals were head restrained, and the implanted optical fiber was connected to a fiber photometry system (RWD life science, no. R820) via a low-fluorescence optical fiber patch cord (outer diameter of 200 μm, 0.37 numerical aperture, length of 2 m). A two-channel model was used in this experiment. The fluorescent signals were simultaneously acquired using light at 470 and 410 nm with time-division multiplexing (*77*). Calcium-dependent signals were recorded at 470 nm, while the signals at 410 nm (an isosbestic point for GCaMP) provided a readout insensitive to calcium concentration (activity-independent signal), which allowed us to monitor and correct motion artifacts. For the *Prrt2*-associated dystonia animal model, calcium signals were recorded over a 10-min duration in each trial. Electrical stimuli, triggered by digital output signals from the fiber photometry system, were delivered to a localized region of the seventh Cb immediately following a 4-min pre-stimulation baseline phase. Animal behaviors were simultaneously recorded by a camera. Each animal underwent three to six trials, with a 1-day recovery period between trials to ensure mice could recover from dystonia attacks. For the KA-induced dystonia animal model, calcium signals were recorded for a 20-min baseline period. Subsequently, KA solution was injected in the seventh Cb and calcium signals were continuously recorded for 2 hours.

Fiber photometry recording in the VL nucleus of the thalamus and RSG

To evaluate neuronal activities in the ventrolateral (VL) nucleus of the thalamus, fiber photometry was used to detect calcium signals in both *Prrt2*-mutant and wild-type mice. In each experimental group, 200 nl of AAV particles (AAV2/9-hSyn-GCaMP6f-WPRE-pA) were injected into the left VL nucleus (AP, −1 mm; ML, −1.2 mm; and DV, −3.3 mm).

To record calcium signals in the RSG, 200 nl of AAV2/9-hSyn-GCaMP6f-WPRE-pA virus was injected into the right RSG (AP, 0.3 mm; ML, −2.92 mm; and DV, −0.9 mm) of *Prrt2*-mutant and wild-type mice.

Subsequently, an optical fiber was implanted, targeting 0.15 mm above the injection site. Following a 1-week recovery period, metal electrodes were implanted into the seventh Cb of the mice. Three weeks after surgery, fiber photometry recordings were conducted in accordance with the aforementioned procedures.

Fiber photometry recording at the axon terminals of Purkinje cells

To investigate calcium activities at the axon terminals of Purkinje cells, fiber photometry was used. A total of 300 nl of AAV2/8-PCP2/L7-GCaMP6f-WPRE-pA virus was injected into the fourth and fifth Cbs (AP, −6.36 mm; ML, −2 mm; and DV, −0.45 mm) in both *Prrt2*-mutant and wild-type mice. For control, the same volume of AAV2/8-

PCP2/L7-EGFP-WPRE-pA virus was injected into the fourth and fifth Cbs of *Prrt2*-mutant mice. Subsequently, an optical fiber was implanted into the IN (AP, −6.36 mm; ML, −1.5 mm; and DV, −2.3 mm) to monitor calcium signals from the axon terminals of Purkinje cells. One week following the viral delivery and optical fiber implantation, metal electrodes were implanted into the seventh Cb according to the procedures outlined in the electrostimulation section. Fiber photometry recordings were performed 3 weeks after virus injection, following previously described methodologies.

Optogenetic activation of DCN

To investigate the involvement of distinct neuronal populations within the DCN in dystonic behaviors, optogenetic manipulation experiments were conducted. For the stimulation of DCN glutamatergic neurons, 200 nl of AAV particles [AAV2/9-EF1α-DIO-hChR2(H134R)-mCherry-WPRE-pA or AAV2/9-hEF1α-DIO-EGFP-WPRE-pA] were injected into the right IN (AP, −6.36 mm; ML, 1.5 mm; and DV, −2.45 mm) of *vGlut2-cre* mice. Similarly, for the stimulation of DCN glycinergic neurons, 200 nl of AAV particles were injected into the right fastigial nucleus (AP, −6.48 mm; ML, 0.95 mm; and DV, −2.45 mm) of *GlyT2-cre* mice. In the case of manipulating DCN GABAergic IO-projecting neurons, 300 nl of AAV particles were injected into the right interposed and dentate nuclei (AP, −6 mm; ML, 2.15 mm; and DV, −2.45 mm), and, simultaneously, 200 nl of AAV particles (scAAV2/2Retro-hSyn-Cre-pA) were injected into the left IO (AP, −6.96 mm; ML, −0.38 mm; and DV, −5.5 mm) of wild-type mice.

After a recovery period of 2 to 3 weeks, optogenetic stimulation was executed in freely moving mice. A laser (ADR-700A, Shanghai Laser & Optics Century Co. Ltd.) was used to generate 473-nm light, which was transmitted to the target region in the DCN through a patch cable. The end of the patch cable was connected to the mice by a fiber cannula previously implanted. Continuous or pulsed blue light (10-ms pulse width at 30 Hz), with an approximate power of 4 mW at the fiber tip, was administered to the free-moving mice for a duration of 20 s. We selected a 20-s stimulation duration to mimic the sustained calcium signal increase in DCN neurons observed during dystonia and minimize potential damage from continuous light exposure. It is worth noting that continuous stimulation may cause initial excitation followed by depolarization block in DCN neurons (*78*), mirroring the responses of the DCN neurons observed in *Prrt2*-mutant mice during dystonic episodes (*17*). Concurrently, the behavioral responses of the mice were recorded with a camera.

Optogenetic activation of RSG

To examine the role of RSG neurons in dystonic behaviors, 200 nl of AAV2/9-hSyn-hChR2(H134R)-mCherry-WPRE-pA virus was injected into the right RSG (AP, 0.3 mm; ML, −2.92 mm; and DV, −0.9 mm) of wild-type mice. An optical fiber was then implanted 0.2 mm above the injection site. Optogenetic stimulation was conducted 3 weeks postinjection using previously established protocols.

Optogenetic inhibition of Purkinje cells

To investigate whether reduced Purkinje cell output contributes to dystonic episodes, optogenetic manipulation experiments were performed. To achieve large-scale inhibition of Purkinje cells, AAV2/9-PCP2/L7-stGtACR2-mCherry-WPRE-pA virus (200 nl per site) was injected into the fourth to eighth Cbs at depths of 0.5 and 1 mm. A glass window (1.8 mm in diameter) was positioned over the brain surface, covering portions of the sixth to eighth Cbs. Three weeks postinjection, mice were head restrained, and continuous blue light (14 mW, 20 s) was delivered via a wide-field microscope to inhibit the targeted neurons. Behavioral responses were simultaneously recorded using a camera.

Open-field test

To evaluate locomotor activity, the open-field test was conducted 3 weeks after injection of taCasp3- or mCherry-encoding AAV particles. Mice were individually placed in a square arena (40 cm by 40 cm by 60 cm) and allowed to explore freely for 10 min. Their movements were recorded via an overhead camera connected to the EthoVision XT11.5 tracking system (Noldus), which automatically quantified the total distance traveled using its analysis software.

Rotarod

To assess motor coordination and balance, a rotarod apparatus (Ugo Basile, Italy) was used 3 weeks after delivery of taCasp3- or mCherry-encoding AAV particles. Mice were placed on a rotating rod starting at a speed of 4 revolutions per minute (rpm), which gradually increased to 40 rpm over 5 min. The latency to fall, defined as the time the mouse remained on the rotarod without falling, was recorded for each trial. Mice underwent a single day of training on the apparatus, followed by testing on the subsequent day.

Beam walking

Motor coordination was assessed via beam walking test at 3 weeks after injection of AAV particles encoding taCasp3 or mCherry. The apparatus consisted of a horizontal wooden beam (1 m in length, 15 mm in diameter), elevated 50 cm above a thick blanket to cushion any falls. A black box was placed at the end of the beam, serving as a safe zone for the mice. Before testing, the mice were habituated to the beam by allowing free exploration for 5 min daily over 2 consecutive days. On the day of testing, each mouse was placed at the starting point of the beam, and the time taken to reach the black box was recorded. Each mouse completed two trials, with a 5-min rest between trials to minimize fatigue. All sessions were video recorded for later analysis. The average latency to cross the beam was calculated from the two trials for each mouse.

Behavioral analyses

Behavior observations were monitored and recorded using a video camera (MV-SUA502C-T, MindVision Technology) at a frame rate of 30 frames per second (fps). Mice were acclimated to the custom-built head plate holder for 30 min daily over 3 days before behavioral tests. Dystonia attacks were defined according to established criteria in previous studies (*17*). In brief, the onset of an attack was identified when dystonic behaviors persisted for more than 5 s. The termination of an attack was determined when the mice returned to normal posture. In this study, dystonic behaviors were systematically identified by the presence of any of the following specific abnormal movements or postures, which include rigid forelimbs or prolonged elevation of the forelimbs, held slowly raised and sustained in mid-air; persistent backward stretching of the ears, remaining tightly pressed against the skin; elongated trunk posture, with the abdomen close to the ground and sometimes the back noticeably arched; prolonged elevation or excessive extension of hindlimbs; and slow, rigid elevation of the tail.

After the application of local stimulation to the cerebellar cortex, *Prrt2*-mutant mice exhibited generalized dystonia, characterized by abnormal postures in five distinct body parts: forelimbs, hindlimbs, tail, trunk, and head. To quantify the severity of dystonia, a rating method was used with a scale ranging from 0 to 5: A score of 0 indicates no dystonic movements; 1 represents dystonic movements in one body part; 2 in two parts; 3 in three parts; 4 in four parts; and 5 indicates dystonia affecting all five parts of the body.

To ensure objectivity and reduce potential bias, the behavioral assessments focusing on the occurrence and severity of dystonia were performed by experimenters who were blind to the conditions of the mice, including the genotype and the specific types of AAV virus injected.

In optogenetic stimulation experiments, behavior is classified as dystonia-like if it resembles one observed in *Prrt2*-mutant mice, occurs exclusively during optogenetic stimulation, and lasts longer than 2 s. For instance, optogenetically induced prolonged elevation of a forelimb or hindlimb in wild-type mice qualifies as dystonia-like behavior under these criteria.

To analyze the severity of the dystonia in kainic acid–treated mice, the same rating method (scale ranging from 0 to 5) used in the *Prrt2*-associated dystonia model was used. Given the distinct characteristics of dystonia attacks in kainic acid–treated mice, where dystonic movements occur repeatedly after injection of kainic acid into the local cerebellar cortex, the cumulative duration of dystonic movements within 30 min (from 40 to 70 min postinjection) was analyzed. This specific time frame was chosen because it typically encompasses the most pronounced dystonic behaviors, consistent with the findings from previous studies (*14*).

Immunofluorescence staining

To assess the expression of GCaMP6f, EGFP, and mCherry, as well as to identify the localization of optical fiber tracks, brain sections from experimental animals were subjected to staining procedures. Mice were anesthetized with pentobarbital (80 mg/kg, intraperitoneal) and then perfused with phosphate-buffered saline (PBS) followed by 4% paraformaldehyde (PFA). Following perfusion, the brain tissues were carefully removed and postfixed in 4% PFA at 4°C for 6 hours. The fixed tissues were then transferred to a 30% sucrose solution (w/v in PBS) at 4°C for dehydration. Coronal sections (25 μm) were cut at −20°C using a Cryostat microtome (Leica, no. CM1950). Subsequently, the brain sections were blocked with blocking solution (3% BSA and 0.3% Triton X-100 in PBS) for 1 hour at room temperature. Following the blocking step, the sections were incubated with Hoechst (1:5000) for 2 hours at room temperature, washed three times in PBS for 5 min each, and mounted onto slides.

To assess the expression of vesicular GABA transporter (vGat), brain slices were prepared as described previously. After the blocking step, the slices were incubated overnight at 4°C with mouse anti-vGat antibody (Abcam, no. ab211534). Following this, the slices were washed three times in PBS and incubated for 2 hours at room temperature with donkey anti-mouse antibody conjugated to Alexa Fluor 647 (Invitrogen, 1:2000) and Hoechst (1:5000). Last, the slices were washed three times in PBS for 5 min each and then mounted onto slides. Fluorescence images were captured using a fluorescence microscope (Olympus, no. VS120) equipped with a 10× objective.

RNAscope

To determine the mRNA level of *vGlut2*, *vGat*, and *GlyT2* in the DCN, in situ hybridization (ISH) was performed on cerebellar slices. Following anesthesia, mice were perfused with diethyl pyrocarbonate (DEPC)–treated PBS and, subsequently, with 4% PFA. The brains were postfixed in 4% PFA at 4°C for 6 hours and then transferred to a 30% DEPC-treated sucrose solution at 4°C for 3 days. Coronal sections (16 μm) were prepared as previously outlined and mounted on SuperFrost Plus slides (Thermo Fisher Scientific, no. 12-550-15). The mouse *vGlut2* probe (Advanced Cell Diagnostics, no. 319171-C2), *vGat* probe (Advanced Cell Diagnostics, no. 319191-C2), and *GlyT2* probe (Advanced Cell Diagnostics, no. 409741-C3) were used in these experiments, and the ISH procedure was executed in accordance with the manufacturer's instructions for RNAscope Multiplex Fluorescent Assays (Advanced Cell Diagnostics, no. 323110). Fluorescence images were captured using a fluorescence microscope (Olympus, no. VS120) equipped with a 10× objective. Glutamatergic neurons in DCN were manually counted. For each animal, images encompassing the three nuclei of the DCN were captured. The average count of DCN neurons from both hemispheres in each image was recorded to evaluate the effects of ablation. The counting of cells was performed by experimenters blinded to the treatment conditions.

Fiber photometry data analysis

The data were analyzed using a customized script written in MATLAB software (MATLAB R2020a), following the method previously described (*77*). Briefly, within individual trials, the fluorescence signals from the 470-nm channel were normalized to the rescaled signals from the 410-nm channel to eliminate the nonspecific responses. The fluorescence change value (z-score) was then calculated as $(F - F_0)/\sigma$, where F_0 and σ were defined as the mean value and SD, respectively, of signal intensity recorded 120 s before electrostimulation in *Prrt2*-associated dystonia animal model and during the 20 min baseline period in the KA-induced dystonia animal model. To determine the onset and cessation of increased calcium signals in each trial, a threshold was set at two times the SD. Data were aligned to the onset of dystonia or the stimulation for analyzing fluorescence dynamics in relation to induced behavior responses. For the control group, the average onset time of dystonic episodes observed in the *Prrt2*-mutant group was adopted as a hypothetical reference point for alignment.

Statistical analysis

The statistical analyses were performed using GraphPad Prism 6 (GraphPad Software Inc., La Jolla, US). To assess the proportion of mice displayed dystonic movements across different groups, we used Fisher's exact test (two sided) to establish statistical significance. To compare dystonia scores, the Mann-Whitney U test was used. To compare the motor coordinate behaviors, attack durations, and the number of three distinct populations of neurons in the DCN between two groups, unpaired Student's t tests were used. Sample sizes were not predetermined using any statistical methods. The results were presented as means ± SEM in all figures. Statistical significance was defined at $P < 0.05$. Further details regarding the statistical tests used and the sample sizes are available in the figure legends.

Supplementary Materials

The PDF file includes:

Figs. S1 to S14
Legends for movies S1 to S6
Legend for data S1

Other Supplementary Material for this manuscript includes the following:
Movies S1 to S6
Data S1

REFERENCES AND NOTES

1. K. Grutz, C. Klein, Dystonia updates: Definition, nomenclature, clinical classification, and etiology. *J. Neural Transm.* **128**, 395–404 (2021).
2. V. S. Kostić, M. Stojanović-Svetel, A. Kacar, Symptomatic dystonias associated with structural brain lesions: Report of 16 cases. *Can. J. Neurol. Sci.* **23**, 53–56 (1996).
3. M. S. Baron, K. D. Chaniary, A. C. Rice, S. M. Shapiro, Multi-neuronal recordings in the Basal Ganglia in normal and dystonic rats. *Front. Syst. Neurosci.* **5**, 67 (2011).
4. A. Nambu, S. Chiken, P. Shashidharan, H. Nishibayashi, M. Ogura, K. Kakishita, S. Tanaka, Y. Tachibana, H. Kita, T. Itakura, Reduced pallidal output causes dystonia. *Front. Syst. Neurosci.* **5**, 89 (2011).
5. S. Chiken, P. Shashidharan, A. Nambu, Cortically evoked long-lasting inhibition of pallidal neurons in a transgenic mouse model of dystonia. *J. Neurosci.* **28**, 13967–13977 (2008).
6. P. Zhuang, Y. Li, M. Hallett, Neuronal activity in the basal ganglia and thalamus in patients with dystonia. *Clin. Neurophysiol.* **115**, 2542–2557 (2004).
7. A. M. Brown, M. E. van der Heijden, H. A. Jinnah, R. V. Sillitoe, Cerebellar dysfunction as a source of dystonic phenotypes in mice. *Cerebellum* **22**, 719–729 (2023).
8. C. Hisatsune, H. Miyamoto, M. Hirono, N. Yamaguchi, T. Sugawara, N. Ogawa, E. Ebisui, T. Ohshima, M. Yamada, T. K. Hensch, M. Hattori, K. Mikoshiba, IP_3R1 deficiency in the cerebellum/brainstem causes basal ganglia-independent dystonia by triggering tonic Purkinje cell firings in mice. *Front. Neural Circuits* **7**, 156 (2013).
9. T. J. Isaksen, L. Kros, N. Vedovato, T. H. Holm, A. Vitenzon, D. C. Gadsby, K. Khodakhah, K. Lykke-Hartmann, Hypothermia-induced dystonia and abnormal cerebellar activity in a mouse model with a single disease-mutation in the sodium-potassium pump. *PLOS Genet.* **13**, e1006763 (2017).
10. R. Fremont, A. Tewari, C. Angueyra, K. Khodakhah, A role for cerebellum in the hereditary dystonia DYT1. *eLife* **6**, e22775 (2017).
11. D. P. Calderon, R. Fremont, F. Kraenzlin, K. Khodakhah, The neural substrates of rapid-onset Dystonia-Parkinsonism. *Nat. Neurosci.* **14**, 357–365 (2011).
12. J. J. White, R. V. Sillitoe, Genetic silencing of olivocerebellar synapses causes dystonia-like behaviour in mice. *Nat. Commun.* **8**, 14912 (2017).
13. R. Fremont, D. P. Calderon, S. Maleki, K. Khodakhah, Abnormal high-frequency burst firing of cerebellar neurons in rapid-onset dystonia-parkinsonism. *J. Neurosci.* **34**, 11723–11732 (2014).
14. C. E. Pizoli, H. A. Jinnah, M. L. Billingsley, E. J. Hess, Abnormal cerebellar signaling induces dystonia in mice. *J. Neurosci.* **22**, 7825–7833 (2002).
15. E. D'Angelo, Physiology of the cerebellum. *Handb. Clin. Neurol.* **154**, 85–108 (2018).
16. J. E. Kim, S. Chae, S. Kim, Y. J. Jung, M. G. Kang, W. Heo, D. Kim, Cerebellar 5HT-2A receptor mediates stress-induced onset of dystonia. *Sci. Adv.* **7**, eabb5735 (2021).
17. B. Lu, S. S. Lou, R. S. Xu, D. L. Kong, R. J. Wu, J. Zhang, L. Zhuang, X. M. Wu, J. Y. He, Z. Y. Wu, Z. Q. Xiong, Cerebellar spreading depolarization mediates paroxysmal movement disorder. *Cell Rep.* **36**, 109743 (2021).
18. B. Coutant, J. L. Frontera, E. Perrin, A. Combes, T. Tarpin, F. Menardy, C. Mailhes-Hamon, S. Perez, B. Degos, L. Venance, C. Lena, D. Popa, Cerebellar stimulation prevents Levodopa-induced dyskinesia in mice and normalizes activity in a motor network. *Nat. Commun.* **13**, 3211 (2022).
19. M. S. LeDoux, J. F. Lorden, J. Meinzen-Derr, Selective elimination of cerebellar output in the genetically dystonic rat. *Brain Res.* **697**, 91–103 (1995).
20. M. S. LeDoux, J. F. Lorden, J. M. Ervin, Cerebellectomy eliminates the motor syndrome of the genetically dystonic rat. *Exp. Neurol.* **120**, 302–310 (1993).
21. J. M. Kebschull, E. B. Richman, N. Ringach, D. Friedmann, E. Albarran, S. S. Kolluru, R. C. Jones, W. E. Allen, Y. Wang, S. W. Cho, H. Zhou, J. B. Ding, H. Y. Chang, K. Deisseroth, S. R. Quake, L. Luo, Cerebellar nuclei evolved by repeatedly duplicating a conserved cell-type set. *Science* **370**, eabd5059 (2020).
22. M. Y. Uusisaari, T. Knopfel, Diversity of neuronal elements and circuitry in the cerebellar nuclei. *Cerebellum* **11**, 420–421 (2012).
23. E. N. Judd, S. M. Lewis, A. L. Person, Diverse inhibitory projections from the cerebellar interposed nucleus. *eLife* **10**, e66231 (2021).
24. M. W. Bagnall, B. Zingg, A. Sakatos, S. H. Moghadam, H. U. Zeilhofer, S. du Lac, Glycinergic projection neurons of the cerebellum. *J. Neurosci.* **29**, 10104–10110 (2009).
25. A. Y. T. Low, A. R. Thanawalla, A. K. K. Yip, J. Kim, K. L. L. Wong, M. Tantra, G. J. Augustine, A. I. Chen, Precision of discrete and rhythmic forelimb movements requires a distinct neuronal subpopulation in the interposed anterior nucleus. *Cell Rep.* **22**, 2322–2333 (2018).
26. Z. Gao, M. Proietti-Onori, Z. Lin, M. M. Ten Brinke, H.-J. Boele, J.-W. Potters, T. J. Ruigrok, F. E. Hoebeek, C. I. De Zeeuw, Excitatory cerebellar nucleocortical circuit provides internal amplification during associative conditioning. *Neuron* **89**, 645–657 (2016).
27. A. Sathyamurthy, A. Barik, C. I. Dobrott, K. J. E. Matson, S. Stoica, R. Pursley, A. T. Chesler, A. J. Levine, Cerebellospinal neurons regulate motor performance and motor learning. *Cell Rep.* **31**, 107595 (2020).
28. G.-H. Tan, Y.-Y. Liu, L. Wang, K. Li, Z.-Q. Zhang, H.-F. Li, Z.-F. Yang, Y. Li, D. Li, M.-Y. Wu, C.-L. Yu, J.-J. Long, R.-C. Chen, L.-X. Li, L.-P. Yin, J.-W. Liu, X.-W. Cheng, Q. Shen, Y.-S. Shu, K. Sakimura, L.-J. Liao, Z.-Y. Wu, Z.-Q. Xiong, PRRT2 deficiency induces paroxysmal kinesigenic dyskinesia by regulating synaptic transmission in cerebellum. *Cell Res.* **28**, 90–110 (2017).
29. C. I. De Zeeuw, S. G. Lisberger, J. L. Raymond, Diversity and dynamism in the cerebellum. *Nat. Neurosci.* **24**, 160–167 (2021).
30. M. Uusisaari, T. Knöpfel, GABAergic synaptic communication in the GABAergic and non-GABAergic cells in the deep cerebellar nuclei. *Neuroscience* **156**, 537–549 (2008).
31. T. M. Teune, J. van der Burg, C. I. de Zeeuw, J. Voogd, T. J. H. Ruigrok, Single Purkinje cell can innervate multiple classes of projection neurons in the cerebellar nuclei of the rat: A light microscopic and ultrastructural triple-tracer study in the rat. *J. Comp. Neurol.* **392**, 164–178 (1998).
32. M. Uusisaari, E. De Schutter, The mysterious microcircuitry of the cerebellar nuclei. *J. Physiol.* **589**, 3441–3457 (2011).
33. C. H. Chen, R. Fremont, E. E. Arteaga-Bracho, K. Khodakhah, Short latency cerebellar modulation of the basal ganglia. *Nat. Neurosci.* **17**, 1767–1775 (2014).
34. S. V. Gornati, C. B. Schäfer, O. H. J. Eelkman Rooda, A. L. Nigg, C. I. De Zeeuw, F. E. Hoebeek, Differentiating cerebellar impact on thalamic nuclei. *Cell Rep.* **23**, 2690–2704 (2018).
35. R. Contreras-Lopez, H. Alatriste-Leon, E. Diaz-Hernandez, J. O. Ramirez-Jarquin, F. Tecuapetla, The deep cerebellar nuclei to striatum disynaptic connection contributes to skilled forelimb movement. *Cell Rep.* **42**, 112000 (2023).
36. B. Sauer, Functional expression of the *cre-lox* site-specific recombination system in the yeast *Saccharomyces cerevisiae*. *Mol. Cell. Biol.* **7**, 2087–2096 (1987).
37. M. L. Streng, M. R. Tetzlaff, E. Krook-Magnuson, Distinct fastigial output channels and their impact on temporal lobe seizures. *J. Neurosci.* **41**, 10091–10107 (2021).
38. O. A. Kim, S. Ohmae, J. F. Medina, A cerebello-olivary signal for negative prediction error is sufficient to cause extinction of associative motor learning. *Nat. Neurosci.* **23**, 1550–1554 (2020).
39. M. Najac, I. M. Raman, Integration of Purkinje cell inhibition by cerebellar nucleo-olivary neurons. *J. Neurosci.* **35**, 544–549 (2015).
40. X. Wang, Z. Liu, M. Angelov, Z. Feng, X. Li, A. Li, Y. Yang, H. Gong, Z. Gao, Excitatory nucleo-olivary pathway shapes cerebellar outputs for motor control. *Nat. Neurosci.* **26**, 1394–1406 (2023).
41. M. J. Wagner, J. Savall, O. Hernandez, G. Mel, H. Inan, O. Rumyantsev, J. Lecoq, T. H. Kim, J. Z. Li, C. Ramakrishnan, K. Deisseroth, L. Luo, S. Ganguli, M. J. Schnitzer, A neural circuit state change underlying skilled movements. *Cell* **184**, 3731–3747.e21 (2021).
42. C. I. de Zeeuw, J. C. Holstege, F. Calkoen, T. J. Ruigrok, J. Voogd, A new combination of WGA-HRP anterograde tracing and GABA immunocytochemistry applied to afferents of the cat inferior olive at the ultrastructural level. *Brain Res.* **447**, 369–375 (1988).
43. K. Nitta, Y. Matsuzaki, A. Konno, H. Hirai, Minimal Purkinje cell-specific PCP2/L7 promoter virally available for rodents and non-human primates. *Mol. Ther. Methods Clin. Dev.* **6**, 159–170 (2017).
44. M. Kneen, J. Farinas, Y. Li, A. S. Verkman, Green fluorescent protein as a noninvasive intracellular pH indicator. *Biophys. J.* **74**, 1591–1599 (1998).
45. X. Sun, Y. Wang, S. Chen, W. Luo, P. Li, Q. Luo, Simultaneous monitoring of intracellular pH changes and hemodynamic response during cortical spreading depression by fluorescence-corrected multimodal optical imaging. *Neuroimage* **57**, 873–884 (2011).
46. C. F. Yang, M. C. Chiang, D. C. Gray, M. Prabhakaran, M. Alvarado, S. A. Juntti, E. K. Unger, J. A. Wells, N. M. Shah, Sexually dimorphic neurons in the ventromedial hypothalamus govern mating in both sexes and aggression in males. *Cell* **153**, 896–909 (2013).
47. A. Asemi-Rad, F. Ghiyamihoor, G. G. Consalez, H. Marzban, Ablation of projection glutamatergic neurons in the lateral cerebellar nuclei alters motor coordination in Vglut2-Cre+ mice. *Cerebellum* **23**, 1313–1320 (2024).
48. A. S. Lee, T. M. Arefin, A. Gubanova, D. N. Stephen, Y. Liu, Z. Lao, A. Krishnamurthy, N. V. De Marco Garcia, D. H. Heck, J. Zhang, A. M. Rajadhyaksha, A. L. Joyner, Cerebellar output neurons can impair non-motor behaviors by altering development of extracerebellar connectivity. *Nat. Commun.* **16**, 1858 (2025).
49. L. J. Ozelius, C. E. Page, C. Klein, J. W. Hewett, M. Mineta, J. Leung, C. Shalish, S. B. Bressman, D. de Leon, M. F. Brin, S. Fahn, D. P. Corey, X. O. Breakefield, The TOR1A (DYT1) gene family and its role in early onset torsion dystonia. *Genomics* **62**, 377–384 (1999).
50. T. Fuchs, R. Saunders-Pullman, I. Masuho, M. S. Luciano, D. Raymond, S. Factor, A. E. Lang, T. W. Liang, R. M. Trosch, S. White, E. Ainehsazan, D. Herve, N. Sharma, M. E. Ehrlich, K. A. Martemyanov, S. B. Bressman, L. J. Ozelius, Mutations in GNAL cause primary torsion dystonia. *Nat. Genet.* **45**, 88–92 (2013).
51. P. de Carvalho Aguiar, K. J. Sweadner, J. T. Penniston, J. Zaremba, L. Liu, M. Caton, G. Linazasoro, M. Borg, M. A. Tijssen, S. B. Bressman, W. B. Dobyns, A. Brashear, L. J. Ozelius, Mutations in the Na^+/K^+-ATPase α3 gene *ATP1A3* are associated with rapid-onset dystonia parkinsonism. *Neuron* **43**, 169–175 (2004).
52. W.-J. Chen, Y. Lin, Z.-Q. Xiong, W. Wei, W. Ni, G.-H. Tan, S.-L. Guo, J. He, Y.-F. Chen, Q.-J. Zhang, H.-F. Li, Y. Lin, S.-X. Murong, J. Xu, N. Wang, Z.-Y. Wu, Exome sequencing

identifies truncating mutations in PRRT2 that cause paroxysmal kinesigenic dyskinesia. *Nat. Genet.* **43**, 1252–1255 (2011).
53. M. Matsumoto, T. Nakagawa, T. Inoue, E. Nagata, K. Tanaka, H. Takano, O. Minowa, J. Kuno, S. Sakakibara, M. Yamada, H. Yoneshima, A. Miyawaki, Y. Fukuuchi, T. Furuichi, H. Okano, K. Mikoshiba, T. Noda, Ataxia and epileptic seizures in mice lacking type 1 inositol 1,4,5-trisphosphate receptor. *Nature* **379**, 168–171 (1996).
54. C. F. Fletcher, A. Tottene, V. A. Lennon, S. M. Wilson, S. J. Dubel, R. Paylor, D. A. Hosford, L. Tessarollo, M. W. McEnery, D. Pietrobon, N. G. Copeland, N. A. Jenkins, Dystonia and cerebellar atrophy in *Cacna1a* null mice lacking P/Q calcium channel activity. *FASEB J.* **15**, 1288–1290 (2001).
55. B. K. Wilson, E. J. Hess, Animal models for dystonia. *Mov. Disord.* **28**, 982–989 (2013).
56. A. M. Pocratsky, F. Nascimento, M. G. Ozyurt, I. J. White, R. Sullivan, B. J. O'Callaghan, C. C. Smith, S. Surana, M. Beato, R. M. Brownstone, Pathophysiology of Dyt1-*Tor1a* dystonia in mice is mediated by spinal neural circuit dysfunction. *Sci. Transl. Med.* **15**, eadg3904 (2023).
57. D. Guehl, P. Burbaud, T. Boraud, B. Bioulac, Bicuculline injections into the rostral and caudal motor thalamus of the monkey induce different types of dystonia. *Eur. J. Neurosci.* **12**, 1033–1037 (2000).
58. H. B. Aïssa, R. W. Sala, E. L. Georgescu Margarint, J. L. Frontera, A. P. Varani, F. Menardy, A. Pelosi, D. Hervé, C. Léna, D. Popa, Functional abnormalities in the cerebello-thalamic pathways in a mouse model of DYT25 dystonia. *eLife* **11**, e79135 (2022).
59. P. Burbaud, B. Bonnet, D. Guehl, A. Lagueny, B. Bioulac, Movement disorders induced by gamma-aminobutyric agonist and antagonist injections into the internal globus pallidus and substantia nigra pars reticulata of the monkey. *Brain Res.* **780**, 102–107 (1998).
60. R. S. Raike, E. J. Hess, H. A. Jinnah, Dystonia and cerebellar degeneration in the leaner mouse mutant. *Brain Res.* **1611**, 56–64 (2015).
61. B. Sterlini, F. Franchi, L. Morinelli, B. Corradi, C. Parodi, M. Albini, A. Bianchi, A. Marte, P. Baldelli, G. Alberini, L. Maragliano, P. Valente, F. Benfenati, A. Corradi, Missense mutations in the membrane domain of PRRT2 affect its interaction with Nav1.2 voltage-gated sodium channels. *Neurobiol. Dis.* **183**, 106177 (2023).
62. F. Fruscione, P. Valente, B. Sterlini, A. Romei, S. Baldassari, M. Fadda, C. Prestigio, G. Giansante, J. Sartorelli, P. Rossi, A. Rubio, A. Gambardella, T. Nieus, V. Broccoli, A. Fassio, P. Baldelli, A. Corradi, F. Zara, F. Benfenati, PRRT2 controls neuronal excitability by negatively modulating Na^+ channel 1.2/1.6 activity. *Brain* **141**, 1000–1016 (2018).
63. E. Manni, L. Petrosini, A century of cerebellar somatotopy: A debated representation. *Nat. Rev. Neurosci.* **5**, 241–249 (2004).
64. K. M. Gruver, J. W. Y. Jiao, E. Fields, S. Song, P. J. Sjöström, A. J. Watt, Structured connectivity in the output of the cerebellar cortex. *Nat. Commun.* **15**, 5563 (2024).
65. A. L. Person, I. M. Raman, Purkinje neuron synchrony elicits time-locked spiking in the cerebellar nuclei. *Nature* **481**, 502–505 (2012).
66. H. Fujita, T. Kodama, S. du Lac, Modular output circuits of the fastigial nucleus for diverse motor and nonmotor functions of the cerebellar vermis. *eLife* **9**, e58613 (2020).
67. N. Ichinohe, F. Mori, K. Shoumura, A di-synaptic projection from the lateral cerebellar nucleus to the laterodorsal part of the striatum via the central lateral nucleus of the thalamus in the rat. *Brain Res.* **880**, 191–197 (2000).
68. T. Schirinzi, G. Sciamanna, N. B. Mercuri, A. Pisani, Dystonia as a network disorder: A concept in evolution. *Curr. Opin. Neurol.* **31**, 498–503 (2018).
69. H. A. Jinnah, V. Neychev, E. J. Hess, The anatomical basis for dystonia: The motor network model. *Tremor. Other Hyperkinet Mov. (N Y)* **7**, 506 (2020).
70. C. N. Prudente, E. J. Hess, H. A. Jinnah, Dystonia as a network disorder: What is the role of the cerebellum? *Neuroscience* **260**, 23–35 (2014).
71. L. Ankri, Z. Husson, K. Pietrajtis, R. Proville, C. Léna, Y. Yarom, S. Dieudonné, M. Y. Uusisaari, A novel inhibitory nucleo-cortical circuit controls cerebellar Golgi cell activity. *eLife* **4**, e06262 (2015).
72. A. H. Gagliuso, E. K. Chapman, G. P. Martinelli, G. R. Holstein, Vestibular neurons with direct projections to the solitary nucleus in the rat. *J. Neurophysiol.* **122**, 512–524 (2019).
73. A. Zwergal, M. Strupp, T. Brandt, J. A. Büttner-Ennever, Parallel ascending vestibular pathways: Anatomical localization and functional specialization. *Ann. N. Y. Acad. Sci.* **1164**, 51–59 (2009).
74. A. K. Horn, The reticular formation. *Prog. Brain Res.* **151**, 127–155 (2006).
75. A. M. Brown, J. J. White, M. E. van der Heijden, J. Zhou, T. Lin, R. V. Sillitoe, Purkinje cell misfiring generates high-amplitude action tremors that are corrected by cerebellar deep brain stimulation. *eLife* **9**, e51928 (2020).
76. M. Uusisaari, T. Knöpfel, GlyT2+ neurons in the lateral cerebellar nucleus. *Cerebellum* **9**, 42–55 (2010).
77. E. Martianova, S. Aronson, C. D. Proulx, Multi-fiber photometry to record neural activity in freely-moving animals. *J. Vis. Exp.*, e60278 (2019).
78. I. M. Raman, A. E. Gustafson, D. Padgett, Ionic currents and spontaneous firing in neurons isolated from the cerebellar nuclei. *J. Neurosci.* **20**, 9004–9016 (2000).

Acknowledgments: We thank faculty members from the Optical Imaging Core Facility of the Center for Excellence in Brain Science and Intelligence Technology (CEBSIT) for assistance with imaging, staff of the Animal Care and Use Committee of CEBSIT for support with animal care, and members of Xiong Lab for technical support and insightful discussions. **Funding:** This work was supported by the National Natural Science Foundation of China, grants 82271269 (B.L.) and 82021001 (Z.-Q.X.); Innovation of Science and Technology 2030-Major Project "platform of nonhuman primate models," 2021ZD02009000 (Z.-Q.X.); Ministry of Science and Technology, 2018YFA0801404 (Z.-Q.X.); and Shanghai Municipal Science and Technology Major Project (Z.-Q.X.).
Author contributions: Conceptualization: Z.-Q.X., B.L., X.-M.W., Z.-Y.W., and Y.-X.Z. Methodology: X.-M.W., B.L., Y.-X.Z., and Z.-Q.X. Investigation: X.-M.W., B.L., J.-Y.H., and Y.-X.Z. Visualization: X.-M.W., B.L., and J.-Y.H. Software: X.-M.W. Formal analysis: X.-M.W., B.L., and J.-Y.H. Validation: X.-M.W., B.L., Y.-X.Z., and J.-Y.H. Funding acquisition: B.L. and Z.-Q.X. Project administration: Z.-Q.X., B.L., and Z.-Y.W. Supervision: Z.-Q.X. and X.-M.W. Writing—original draft: X.-M.W., B.L., Z.-Q.X., and J.-Y.H. Writing—review and editing: X.-M.W., B.L., Z.-Y.W., and Z.-Q.X. **Competing interests:** The authors declare that they have no competing interests. **Data and materials availability:** All data needed to evaluate the conclusions in the paper are present in the paper and/or the Supplementary Materials.

Submitted 15 March 2024
Accepted 8 April 2025
Published 9 May 2025
10.1126/sciadv.adp2377